ELSEVIER

Journal of Volcanology and Geothermal Research 113 (2002) 129–157

Journal of volcanology and geothermal research

www.elsevier.com/locate/jvolgeores

The Oligocene Lund Tuff, Great Basin, USA: a very large volume monotonous intermediate

Larissa L. Maughan [a], Eric H. Christiansen [a,*], Myron G. Best [a], C. Sherman Grommé [b,1], Alan L. Deino [c], David G. Tingey [a]

[a] *Department of Geology, Brigham Young University, Provo, UT 84602, USA*
[b] *U.S. Geological Survey, Menlo Park, CA 94025, USA*
[c] *Berkeley Geochronology Center, Berkeley, CA 94709, USA*

Received 19 August 1999; received in revised form 15 June 2001; accepted 15 June 2001

Abstract

Unusual monotonous intermediate ignimbrites consist of phenocryst-rich dacite that occurs as very large volume (>1000 km^3) deposits that lack systematic compositional zonation, comagmatic rhyolite precursors, and underlying plinian beds. They are distinct from countless, usually smaller volume, zoned rhyolite–dacite–andesite deposits that are conventionally believed to have erupted from magma chambers in which thermal and compositional gradients were established because of sidewall crystallization and associated convective fractionation. Despite their great volume, or because of it, monotonous intermediates have received little attention. Documentation of the stratigraphy, composition, and geologic setting of the Lund Tuff – one of four monotonous intermediate tuffs in the middle-Tertiary Great Basin ignimbrite province – provides insight into its unusual origin and, by implication, the origin of other similar monotonous intermediates.

The Lund Tuff is a single cooling unit with normal magnetic polarity whose volume likely exceeded 3000 km^3. It was emplaced 29.02 ± 0.04 Ma in and around the coeval White Rock caldera which has an unextended north–south diameter of about 50 km. The tuff is monotonous in that its phenocryst assemblage is virtually uniform throughout the deposit: plagioclase $>$ quartz $\approx$ hornblende $>$ biotite $>$ Fe–Ti oxides $\approx$ sanidine $>$ titanite, zircon, and apatite. However, ratios of phenocrysts vary by as much as an order of magnitude in a manner consistent with progressive crystallization in the pre-eruption chamber. A significant range in whole-rock chemical composition (e.g., 63–71 wt% SiO_2) is poorly correlated with phenocryst abundance.

These compositional attributes cannot have been caused wholly by winnowing of glass from phenocrysts during eruption, as has been suggested for the monotonous intermediate Fish Canyon Tuff. Pumice fragments are also crystal-rich, and chemically and mineralogically indistinguishable from bulk tuff. We postulate that convective mixing in a sill-like magma chamber precluded development of a zoned chamber with a rhyolitic top or of a zoned pyroclastic deposit. Chemical variations in the Lund Tuff are consistent with equilibrium crystallization of a parental dacitic magma followed by eruptive mixing of compositionally diverse crystals and high-silica rhyolite vitroclasts during evacuation and emplacement. This model contrasts with the more systematic withdrawal from a bottle-shaped chamber in which sidewall crystallization creates a marked vertical compositional gradient and a substantial volume

[1] Present address: 420 Chaucer St., Palo Alto, CA 94301, USA.

* Corresponding author. Tel.: +1-801-378-2113; fax: +1-801-378-8143.
E-mail address: eric_christiansen@byu.edu (E.H. Christiansen).

0377-0273/02/$ – see front matter
PII: S0377-0273(01)00256-6

of capping-evolved rhyolite magma. Eruption at exceptionally high discharge rates precluded development of an underlying plinian deposit.

The generation of the monotonous intermediate Lund magma and others like it in the middle Tertiary of the western USA reflects an unusually high flux of mantle-derived mafic magma into unusually thick and warm crust above a subducting slab of oceanic lithosphere.

Keywords: monotonous intermediate; crystal-rich dacite; ash-flow tuff; very large volume ignimbrite; magma chamber shape; eruptive mixing; convective mixing; equilibrium crystallization

1. Introduction

Numerous publications over the past three decades have described compositionally zoned ash-flow deposits presumed to have been derived from magma chambers in which convective fractionation was driven by sidewall crystallization. However, Hildreth (1981, p. 10,157) recognized a distinctly different class of ash-flow deposits which he designated as *monotonous intermediates* that are "... mostly phenocryst-rich sheets of large volume but limited compositional range...." He further noted that "These phenocryst-rich intermediate magmas appear to represent the 'dominant volume' from which silicic upper layers sometimes develop within magma chambers." Nonetheless, some magmas appeared to have erupted voluminously without a precursory rhyolite. He indicated this scenario "... may be related ... to system dimensions, crustal thickness, crustal stress distribution, and rate of input of basaltic magma into the roots of the system."

In subsequent decades, these unusual monotonous intermediate ignimbrites have received little attention. Little is known regarding: (1) just how 'monotonous' their compositions really are; (2) the nature of compositional gradients – if any – in the pre-eruption magma chamber; (3) possible overprinting of the primary magmatic characteristics by mixing of crystal and glass clasts during eruption or by their fractionation by winnowing; and (4) the role of chamber attributes and tectonic setting in the origin and evolution of the magmas.

Hildreth (1981) specifically designated cooling units of the Needles Range Formation (now Group) in the Great Basin as monotonous intermediates. The Lund Tuff, which is one of these units, has been studied in an attempt to better understand this intriguing class of ignimbrite.

In this paper, we define a monotonous intermediate tuff as a very large volume (>1000 km^3) deposit of crystal-rich (generally $>25\%$ phenocrysts on a dense rock basis) dacite that lacks conspicuous compositional zonation and an extensive underlying comagmatic rhyolitic precursor. Part of the 'monotonous' designation arises from the uniform appearance of the ignimbrite through intracaldera thicknesses of 2 km or more and diameters of tens of km and outflow sheets to as thick as 500 m covering present areas as much as 50 000 km^2.

This contribution on the Lund Tuff should not be construed as the final word on monotonous intermediate tuffs. Ongoing research in the San Juan volcanic field by P.W. Lipman, M.A. Dungan and associates, in the remote central Andes by S.L. de Silva and others, and in the Great Basin by us will undoubtedly shed additional insights into monotonous intermediates that will test the conclusions presented here.

2. Overview of monotonous intermediate tuffs

2.1. Fish Canyon Tuff

The best known monotonous intermediate is the Fish Canyon Tuff – a crystal-rich dacite emplaced 28 Ma in the San Juan volcanic field (Lipman, 1975; Renne et al., 1998) of southwestern Colorado (Fig. 1). Pumice clasts large enough to separate from the tuff are rare, but the bulk tuff ranges from 65 to 69% SiO_2 and Rb, Sr, and Ba vary by a factor of about 1.3. The tuff has 37–54% phenocrysts of plagioclase > sanidine ≈ bioti-

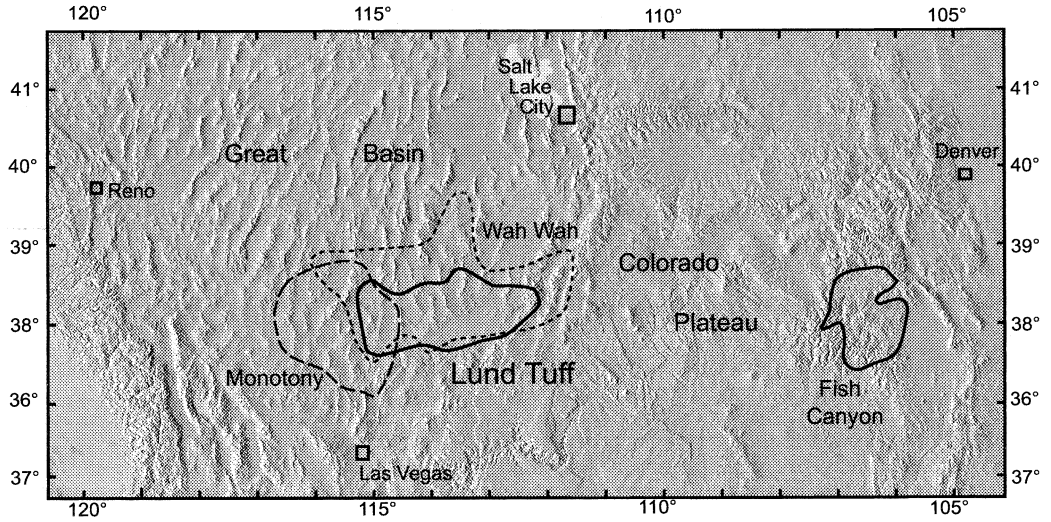

Fig. 1. Shaded relief map of the middle Rocky Mountains (west of Denver), Colorado Plateaus, and Great Basin showing outlines of monotonous intermediate tuffs. For clarity, the Cottonwood Wash Tuff, which is overlapped by the Lund and Wah Wah Springs outflow sheets in the Great Basin, has been omitted. Base map courtesy of Ken Perry, Chalk Butte Inc.

te > hornblende ≈ quartz > Fe–Ti oxides > titanite, apatite, and zircon. Whitney and Stormer (1985) concluded that (p. 757) "The Fish Canyon tuff magma was extremely homogeneous in major and trace element abundances, and phenocryst assemblage. The main mechanism responsible for minor chemical differences [in the tuff] is variation in the phenocryst to groundmass ratio probably caused by glass winnowing during eruption" and that (p. 745) "There is no evidence for a regular chemical stratification in the magma chamber." Lipman et al. (1997) and Lipman (2000) reaffirmed the compositional uniformity of the Fish Canyon and increased the estimated volume from about 3000 to about 5000 km^3. The Fish Canyon lacks a plinian precursor, rhyolitic or otherwise, but pyroclastic surge deposits are locally present. The source caldera is about 35×75 km.

2.2. Central Andes deposits

Reconnaissance work on the 2.2 Ma Cerro Galan ignimbrite at the southern end of the high Altiplano–Puna in the central Andes by Francis et al. (1989) suggests it is a monotonous intermediate. It has a minimum volume of 1000 km^3 and extends as much as 100 km in radial directions from the 30×50 km resurgent caldera. A plinian ash-fall precursor is absent. Phenocrysts are abundant (41–53% of whole rock), lithic and pumice clasts are rare, Rb, Sr, and Ba vary by a factor of nearly 2, and pumice clasts range from 66 to 70 wt% SiO_2. Francis et al. (1989) conclude that the ignimbrite was derived from a weakly zoned, or perhaps only a somewhat heterogeneous, magma chamber.

2.3. Monotonous intermediates of the Great Basin

The middle-Tertiary Great Basin ash-flow province (Fig. 1; Best et al., 1989b, 1993) developed during the great ignimbrite flareup that accompanied subduction of an oceanic plate beneath western North America (Severinghaus and Atwater, 1990). An arc signature (calc-alkaline rocks with negative Nb and Ti anomalies on normalized trace element diagrams) is evident in the flareup tuffs and contemporaneous lava flows.

The Great Basin harbors at least four monotonous intermediates. In the volcanic field in and around the Indian Peak caldera complex (Best et al., 1989a), three intermediate tuffs in the Needles Range Group, in ascending order, are the Cotton-

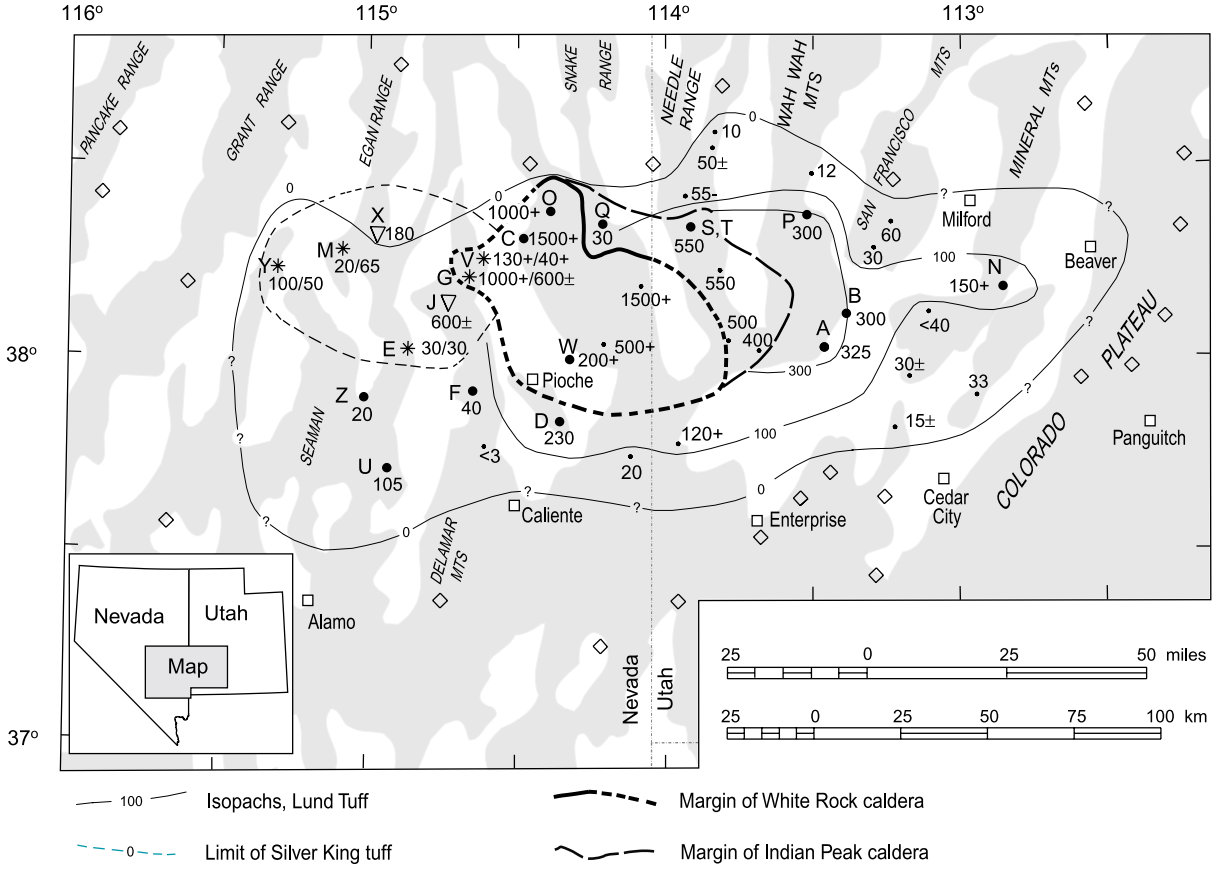

Fig. 2. Map of part of Great Basin in Nevada and Utah showing extent and thickness of the Lund Tuff and its White Rock caldera source (as well as the older Silver King tuff). Zero isopach of the Lund Tuff shown queried where its location is conjectural. Margin of the White Rock caldera shown as a bold solid line where mapped and as a dashed line where known only approximately (Best et al., 1989a). A preserved segment of the older Indian Peak caldera is shown by dashed line. Sample localities (detailed in Appendix A[2]): Closed circles, only Lund Tuff present; inverted triangles, only Silver King tuff present; asterisks, both units present. Localities where stratigraphic thicknesses are known shown as small filled circles. Thickness in meters; where both units are present, thickness of Lund/thickness of Silver King. Locations where the Lund Tuff is known to be absent shown as open diamonds.

wood Wash (emplaced at 31.0 Ma), Wah Wah Springs (30.2), and Lund (29.0) – the subject of this paper. In the Central Nevada volcanic field is the Monotony (27.5) (Ekren et al., 1971; Phillips, 1989).

Where exposed, bedded pyroclastic surge deposits are <1 m thick and plinian fallout deposits are apparently absent beneath the ignimbrites. There are no significant volumes of underlying rhyolite that could represent an erupted differentiate capping the dacitic 'dominant volume' of the pre-eruption magma chamber. The Wah Wah Springs Tuff lies directly on the Cottonwood Wash with no intervening rhyolite. Bedded, well-sorted sandstone a few meters thick separates Cottonwood Wash and Lund tuffs from underlying low-silica rhyolite tuffs. In addition to the implied time breaks, the compositions of the rhyolite tuffs render them improbable differentiates of the dacite magmas. The rhyolite tuffs are

[2] See Electronic Supplements on http://www.elsevier.com/locate/jvolgeores

low-silica (~71 wt% SiO_2) and contain 10–15% phenocrysts of chiefly plagioclase and biotite with very little quartz and sanidine; such rhyolite magma would not be expected as a differentiate from dacite magma in which the melt was high-silica (>76 wt% SiO_2; see below) and in equilibrium with sanidine and quartz. The only rhyolite deposits underlying the Monotony are tuffs more than 1.5 Myr older.

Cognate pumice clasts in monotonous intermediates are typically inconspicuous; where present, they are generally intensely compacted lapilli in densely welded tuff.

The four monotonous intermediates in the Great Basin were emplaced during a brief 3.5 Myr episode (31.0–27.5 Ma) within the much longer ignimbrite flareup (34–17 Ma) but comprise a volume nearly that of the rhyolite tuffs that dominate the remainder of the flareup (Best et al., 1989b; Best and Christiansen, 1991). The brevity of this unique monotonous intermediate burst is all the more remarkable when it is realized that volcanism in western North America related to subduction has persisted diachronously up to the present since at least the early Mesozoic. Large volumes of lavas (chiefly andesitic, no basalt) were extruded before and within several Myr after the monotonous intermediate burst in the Great Basin (Best and Christiansen, 1991; Barr, 1993).

Despite assertions of regional tectonic extension during the ignimbrite flareup, we find no direct stratigraphic evidence for such activity in the outflow areas surrounding the Central Nevada and Indian Peak caldera complexes (Best and Christiansen, 1991). Outflow stratigraphic sections consist of tuff sheet lying conformably upon tuff sheet separated only by local fine-grained sedimentary deposits and intervening lava flows. Coarse epiclastic deposits of volcanic detritus between outflow sheets, which would be expected during regional synvolcanic extension, are notably absent, as are angular discordances, which only occur in the vicinity of the local piles of lava. Beginning about 23 Ma, the ignimbrite flareup waned, nonarc geochemical signatures appeared, volcanism became increasingly bimodal, and widespread extension created the well-known basin and range structure and topography.

Table 1
Paleomagnetic directions in the Lund Tuff and Silver King tuff

Site	Latitude	Longitude	N	Tr.	R	k	α_{95}	I	D	PLA	PLO
Lund Tuff											
De	37.844	245.601	7	L	6.97220	215.8	4.1	65.2	347.1	76.7	204.6
Dw	37.832	245.641	7	L	6.99412	1020.0	1.9	51.3	326.4	62.0	153.8
E	38.020	245.136	7	L	6.98269	346.5	3.3	55.5	320.7	58.8	163.9
F	37.913	245.348	8	L	7.96504	200.2	3.9	56.1	323.3	60.9	164.4
O	38.377	245.608	8	L	7.99408	1181.7	1.6	62.1	311.5	53.5	179.3
P	38.472	246.531	10	40	9.97861	420.7	2.4	46.4	329.5	62.4	142.6
U	37.708	245.065	8	L	7.98671	526.9	2.4	55.3	320.4	58.5	164.0
Z	37.897	244.981	8	L	7.99369	1109.2	1.7	55.0	324.3	61.4	161.3
Silver King Tuff											
E	38.021	245.135	8	L	7.97037	236.2	3.6	−59.4	127.5	−49.8	355.2
Jb	38.143	245.270	8	L	7.97227	252.4	3.5	−69.5	102.4	−36.6	18.5
Ja	38.144	245.270	8	L	7.92982	99.7	5.8	−72.4	140.1	−57.6	25.2
X	38.319	245.034	8	L	7.98657	521.2	2.4	−69.8	108.8	−40.5	17.5
Y	38.229	244.693	8	L	7.99767	3003.3	1.0	−77.4	115.0	−35.7	37.6
Yv	38.231	244.693	6	L	5.98460	324.7	3.7	−73.4	142.2	−58.2	28.1

Site, site designation from Fig. 2. (e, eastern fault block; w, western fault block; v, vitrophyre; a, b, lower and upper parts of unit, respectively). Latitude and longitude of site (degrees). N, number of oriented cores at site. Tr., magnetic cleaning treatment (L, best-fit lines (Kirschvink, 1980); 40, blanket demagnetization at 40 mT). R, sum of N unit vectors. k, Fisher (1953) concentration parameter. α_{95}, radius of 95% confidence cone (Fisher, 1953). I, inclination (degrees, negative upward signifying reversed polarity). D, declination (degrees eastward). PLA, latitude of virtual geomagnetic pole (degrees, negative in southern hemisphere). PLO, longitude of virtual paleomagnetic pole (degrees eastward).

3. Stratigraphy of the Lund Tuff

3.1. Recognition of an older ignimbrite beneath the Lund Tuff

In order to understand the nature and origin of the Lund Tuff, it is mandatory to have a clear understanding of what is and what is not part of the tuff. This correlation problem is compounded by the superficial similarities among the sequentially emplaced sheets of the Indian Peak volcanic field. Recent work shows that some deposits mapped as part of the Lund Tuff are in fact a separate ignimbrite, herein informally named the Silver King tuff. This crystal-rich titanite-bearing dacite underlies the northwestern part of the Lund Tuff (Fig. 2) and has an estimated volume of about 200 km^3. It is reversely magnetized, unlike the Lund (Table 1; Fig. 3). Ekren and Page (1995) mapped a stratigraphic sequence in which the two cooling units are separated by a thin andesitic lava flow at locality E in Fig. 2. This figure and table indicate four additional sites where both cooling units have been found and sampled. Precise single crystal $^{40}Ar/^{39}Ar$ analyses (Table 2) disclose an age difference of about 0.2 Myr between the two units. Maughan (1996) demonstrated that the Silver King tuff is distinct from the Lund Tuff in other ways as well: (a) it has less than 6% hornblende phenocrysts; (b) it has lower P_2O_5, Fe_2O_3, Sc, V, and Cr and higher SiO_2 at similar TiO_2; (c) mafic phenocrysts have compositions different from those in the Lund Tuff. These data show no possibility of a closed system lineal descent of the Lund magma from the Silver King magma. No source caldera for the Silver King tuff has been found.

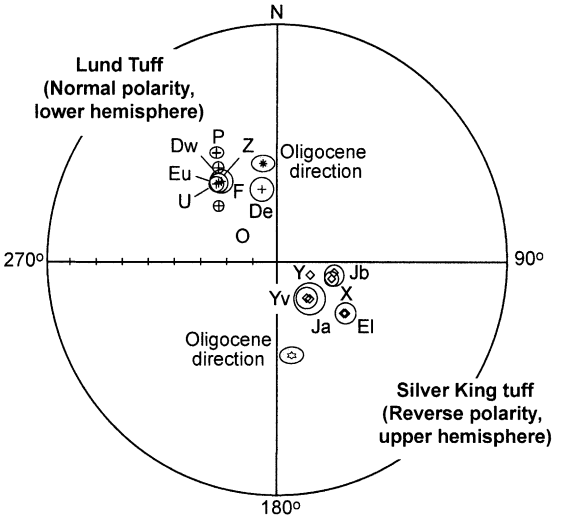

Fig. 3. Equal-area projection of site-mean paleomagnetic directions in the Silver King tuff and Lund Tuff. Circles are 95% confidence radii centered on mean directions (Fisher, 1953). Labels correspond to Fig. 2 (and Appendix A). Asterisk (normal polarity) and open star (reversed polarity) with 95% confidence ellipses are Oligocene paleomagnetic axial dipole field directions expected for eastern Nevada, calculated from North America reference dipole of Diehl et al. (1983). Note that the data for site P (N13 in Grommé et al., 1972) was used in their compilation.

3.2. Paleomagnetism

Oriented cores were collected at 14 sites in the Lund and Silver King units; paleomagnetic results are shown in Table 1 and Fig. 3. Data for one site (P in Table 1) were previously reported by Grommé et al. (1972, site N13) when it was erroneously thought to be the Wah Wah Springs Tuff. Standard methods were used for the field collection and laboratory measurements (Grommé et al., 1972; Scott et al., 1995). We have paleomagnetic data from one locality (E in Fig. 2) where the Lund Tuff and the underlying Silver King are in unquestionable stratigraphic order. Fig. 3 shows the reverse and normal polarity of the Silver King and Lund Tuff, respectively. Within each polarity group, the between-site angular differences may be due in part to geomagnetic secular variation, but more likely are the result of imperfect knowledge of original horizontal at the times of cooling and acquisition of thermoremanent magnetization (Grommé et al., 1972). For both polarity groups the differences between the tuff paleomagnetic directions and the predicted directions are well within the normal range of geomagnetic secular variation.

3.3. $^{40}Ar/^{39}Ar$ chronology

Sanidine phenocrysts extracted from two samples of the Lund Tuff and two samples of the

Table 2
$^{40}Ar/^{39}Ar$ data on sanidines from the Lund Tuff and the Silver King tuff

Unit Sample #	Lab ID#	$J \pm 1\sigma$	n/n_0	Ca/K $\pm 1\sigma$	$^{40}Ar^*/^{39}Ar \pm 1\sigma$	MSWD	Age (Ma $\pm 1\sigma$)
Lund Tuff							
MIN-8V	7729	0.01691 ± 0.00002	8/9	0.0096 ± 0.0062	0.9589 ± 0.0008	0.9	29.02 ± 0.05
WATER-1-22M	21020	0.01043 ± 0.00001	10/10	0.0127 ± 0.0010	1.5547 ± 0.0013	1.2	29.03 ± 0.05
Silver King tuff							
SILVRWL-1E	7726	0.01695 ± 0.00002	9/9	0.0064 ± 0.0031	0.9628 ± 0.0008	0.7	29.21 ± 0.04
WATERNE-1C	7727	0.01695 ± 0.00002	8/9	0.0054 ± 0.0027	0.9633 ± 0.0008	0.5	29.22 ± 0.04

J is the neutron fluence parameter determined by analysis of a standard of known age co-irradiated with the unknowns. The samples were irradiated in two batches. The first batch (samples MIN-8V, SILVRWL-1E, and WATERNE-1C) was irradiated for 60 h in the Cd-shielded CLICIT facility of the Oregon State University TRIGA reactor, using 22.782 Ma old sanidine from the Pahranagat tuff as the age standard (Best et al., 1995 modified for revised age of Fish Canyon Tuff of 28.02 Ma as per Renne et al., 1998). The second batch (sample WATER-1-22M) was irradiated in the same facility for 40 h, using 27.84 Ma old sanidine from the Fish Canyon Tuff as the standard (Renne et al., 1998). n/n_0 refers to the number of individual grain analyses accepted for calculation of weighted mean $^{40}Ar^*/^{39}Ar$ calculation, over the total number of analyses performed; grains falling more than two standard deviations beyond the overall weighted mean age were rejected. MSWD is the mean sum of weighted deviates of the individual ages. Error in age is 1σ standard error of the mean, and incorporates error in *J*. See Fig. 2 and Appendix for locations of samples.

Silver King tuff were dated by the single-crystal, laser-fusion $^{40}Ar/^{39}Ar$ method. Details of the methodology have been presented earlier (Best et al., 1995). Results are summarized in Table 2. The dating results are straightforward; within-sample replicate analyses have simple, gaussian-like distributions (reflected in mean sums of weighted deviates near or less than 1), and between-sample reproducibility is on the order of 10 ka. The weighted mean age for the Lund Tuff is 29.02 ± 0.04 Ma and that for the Silver King tuff is 29.22 ± 0.03 Ma, a difference of 200 ka.

3.4. Source caldera and dimensions of the Lund Tuff

Definition of the northern and eastern margins of the White Rock caldera (Fig. 2) that was the source of the Lund Tuff is based on thick accumulations of densely welded, pumice-poor tuff comprising a compound cooling unit. Intercalated lenses of monolithologic breccia of Paleozoic carbonate rock within the intracaldera tuff are interpreted to have formed by collapse of the unstable wall of the subsiding caldera (Best et al., 1989a,b). In the northern Wilson Creek Range, the thickness of the intracaldera facies of the Lund Tuff ranges from 1 km to possibly more than 2.5 km. In the Fairview Peak Range (Best et al., 1998) and in the central Needle Range it is as much as 1 km thick. Elsewhere the caldera is defined by thinner remnants of intracaldera tuffs and by a Bouguer gravity signature (Best et al., 1989a).

Calculation of the eruptive volume of any ash-flow deposit in the Great Basin depends critically on the amount of crustal extension after emplacement. But extension was heterogeneous, differing significantly between different structural domains, and in some domains apparently occurred before the ignimbrite flareup as well as afterward. Detailed evaluation of post-Lund extension in the area of the tuff has not been made. However, in an east–west transect now 400 km long between about 39°N and 40°N (just north of the Lund outflow sheet), Smith et al. (1991) determined an average extension of 55%. The amount of post-Lund extension may be less than this total value.

Using lower and upper limits of 30 and 70% extension and thicknesses shown in Fig. 2, volumes of the Lund outflow sheet are 1200 and 1000 km^3 and for the intracaldera accumulation 2400–1900 km^3, respectively. The volume of the tuff within the White Rock caldera is a minimum because a uniform thickness of only 1 km was assumed. The eruptive volume of the Lund Tuff was, therefore, likely >3000 km^3. The uncertain-

Table 3
Chemical and modal composition of selected samples of the Lund Tuff

Sample number	COYOT-1E Tuff	HOR-11 Tuff	LAM-5V Vitrophyre	MIN-8V Vitrophyre	PAHRC-2C Tuff	ROSE-1 Tuff	WATER-1-34M Tuff	MLLR-6-65-1A Pumice	MLLR-6-65-1PE Pumice
wt%									
SiO_2	65.30	68.34	66.43	64.81	66.65	64.47	69.98	66.29	66.65
TiO_2	0.68	0.57	0.68	0.71	0.70	0.77	0.48	0.68	0.62
Al_2O_3	15.71	14.92	15.19	15.81	15.48	16.23	14.44	15.68	15.25
Fe_2O_3	4.99	4.33	5.03	5.37	4.95	5.65	3.59	4.99	4.76
MnO	0.08	0.05	0.09	0.09	0.07	0.07	0.07	0.09	0.08
MgO	1.41	1.39	2.02	2.06	1.61	1.67	0.99	1.41	1.46
CaO	4.82	3.85	4.19	4.87	3.99	4.56	2.78	3.87	3.67
Na_2O	2.80	2.82	3.21	2.88	2.35	3.15	2.88	2.92	3.09
K_2O	4.03	3.57	2.95	3.20	4.00	3.19	4.62	3.87	4.15
P_2O_5	0.19	0.16	0.22	0.21	0.21	0.24	0.16	0.20	0.27
LOI	1.17	0.86	2.02	1.38	2.25	0.80	1.02	0.76	0.92
Anal. total	99.41	99.74	99.69	99.68	99.30	99.33	99.83	99.54	99.70
ppm									
F	664	684	1042	964	783	962	651	698	948
S	94	141	133	125	151	94	69	75	83
Cl	129	134	271	261	135	153	54	122	142
Sc	11	8	12	12	11	14	8	11	11
V	84	76	97	105	102	109	59	89	74
Cr	15	14	16	20	20	19	5	17	15
Ni	15	14	14	16	15	19	3	15	17
Cu	13	11	14	18	16	15	16	15	21
Zn	56	51	62	67	62	70	53	57	50
Ga	19	18	19	21	19	21	18	19	18
Rb	110	98	119	100	138	96	167	116	126
Sr	552	537	545	606	524	640	378	565	586
Y	22	21	23	23	22	21	17	23	21
Zr	206	194	229	232	226	227	216	216	222
Nb	12	12	12	11	10	13	14	10	10
Ba	933	982	950	896	820	901	874	981	1006
La	42	42	57	50	49	46	63		50
Ce	95	101	108	107	116	101	104	131	103
Nd	37	38	43	41	45	40	34	49	40
Sm	7	7	8	7	8	6	9	8	8
Pb	20	19	24	21	23	20	27	25	24
Th	18	17	20	18	20	16	34	21	21
U	5	4	6	6	6	4	4	4	4
Modal proportions									
Plagioclase	60.6	52.4	57.7	62.0	58.3	59.2	53.1	58.2	57.6
Quartz	10.9	17.7	5.0	5.7	2.9	17.3	11.1	16.9	12.2
Sanidine	2.3	9.7	0.0	0.2	0.0	0.0	3.3	0.0	3.3
Biotite	9.1	9.9	8.2	9.4	11.1	8.3	16.3	10.7	6.4
Hornblende	12.1	7.7	21.4	19.0	21.6	12.7	10.6	11.6	16.8
Clinopyroxene					0.5				0.2
Opaques	4.6	2.1	7.0	3.5	5.6	2.5	5.1	2.6	3.4
Titanite	0.4	0.5	0.7	0.2	Trace	Trace	0.5	Trace	0.1
Tot Pheno	40.6	56.5	41.9	51.4	33.4	56.5	22.1	55.4	54.2

Oxide values in wt% have been recalculated to 100% on a volatile-free basis. Anal. Total = actual analytical total. LOI = loss on ignition. Trace element concentrations are given in ppm. Modal proportions relative to phenocrysts (vol%) except for Total phenocrysts, which is given compared to dense rock.

ties in the correction for extension are larger than the correction to the dense rock equivalent volume, but based on a measured average tuff density of 2.3 g/cm^3, the volume would be reduced by about 10%. The disparity in relative intracaldera and outflow volumes, approximately equal for some large ignimbrites (Lipman, 1997), probably reflects the fact that initial Lund ash flows were erupted within an older caldera formed during eruption of the Wah Wah Springs ash flows. Sub-

sequent collapse of the White Rock caldera obliterated most of this older depression (Best et al., 1989a).

4. Petrography and composition of the Lund Tuff

The Lund Tuff is typically moderately to densely welded and contains abundant phenocrysts of plagioclase, lesser quartz, hornblende, biotite, minor sanidine, magnetite, and trace amounts of ilmenite, apatite, and zircon. Trace amounts of wedge-shaped titanite grains 1–1.5 mm long are present in most samples and are the most obvious difference between the Lund Tuff and the three otherwise similar large monotonous intermediate tuffs in the Great Basin. In three Lund samples, sparse orthopyroxene (partially altered to hornblende and Fe–Ti oxides) is probably xenocrystic. Phenoclasts (Best and Christiansen, 1997) of plagioclase are commonly <1 mm but range to as much as 3.5 mm and contain inclusions of, in decreasing order of abundance, apatite, magnetite, biotite, hornblende, ilmenite, and zircon; some inclusion-rich cores of plagioclases may be restite. Embayed phenoclasts of quartz are as much as 4 mm in diameter and rarely less than 1 mm in diameter; the lack of strain and healed microcracks in quartz grains suggest none are xenocrysts or restite. Phenocrysts of biotite are common and most have inclusions of apatite, magnetite, plagioclase, hornblende, ilmenite, and zircon. A similar suite and proportions of inclusions are found in hornblende phenocrysts, except biotite is present instead of hornblende. Electron microprobe analyses indicate a lack of compositional zoning in the mafic phenocrysts.

Lithic clasts are virtually nonexistent in the Lund Tuff. Cognate pumice clasts are uncommon in the intracaldera facies but more widespread in the outflow sheet. Unfortunately, their generally small (lapilli) size and dense compaction precludes extraction for laboratory analyses. Only five cognate inclusions (from two sites) were of sufficient size for study. The mineral assemblage in these phenocryst-rich inclusions is identical to the bulk tuff.

4.1. Modal composition

Modal analyses of thin sections show that the total phenocryst proportions in the tuff are typically high, with a median of 47 vol% phenocrysts, an average of $43\% \pm 12$ (1 standard deviation), and a range of 14–56%, all on a dense rock basis. Pumice clasts are also rich in phenocrysts with an average of $52 \pm 4\%$. Samples from the western part of the tuff sheet, especially those collected from the Y section, have fewer total phenocrysts. These anomalous samples are considered further below.

Within these crystal-rich rocks, there are substantial variations in proportions of plagioclase (64–48% of total phenocrysts), sanidine (10–0%), quartz (26–2%), biotite (20–6%), hornblende (22–8%), and opaques (essentially Fe–Ti oxides, 8–2%) (Table 3; Figs. 4 and 5). Unlike many zoned rhyolitic tuff deposits, no major crystalline phase appears or disappears vertically or laterally through the Lund Tuff. Some samples contain no sanidine but its absence is not systematic spatially in the deposit. However, some phenocryst

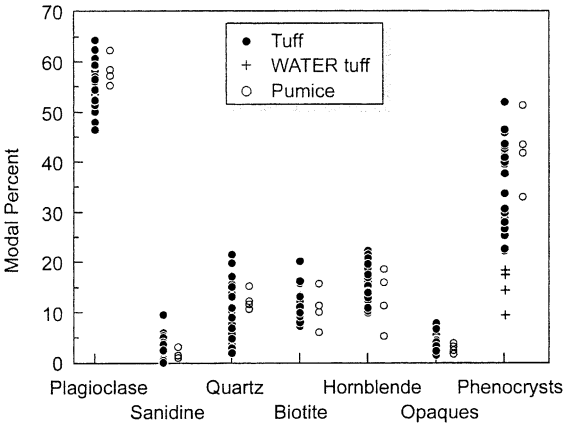

Fig. 4. Modal proportions of phenocrysts in the Lund Tuff and its pumice clasts (accessory titanite, apatite, and zircon not shown). Modal % of individual phase, e.g., plagioclase, is with respect to total phenocrysts whereas modal % of phenocrysts is with respect to whole rock. Pumice clasts are similar to bulk tuff samples. Phenocryst-poor samples are from the WATER section (site Y in Fig. 2) in the distal western part of the outflow sheet, but individual phase proportions are not distinguishable from other samples of the tuff.

ratios vary by more than an order of magnitude, including hornblende/quartz (11–0.3), plagioclase/quartz (32–2), and opaque minerals/quartz (1.75–0.15). The felsic/mafic phenocryst ratio varies between 5 and 1. Quartz varies antithetically with hornblende (Fig. 5), plagioclase, opaque grains (Fe–Ti oxides), and biotite but sympathetically with sanidine and total phenocrysts (Fig. 5). Some workers have suggested that phenocryst ratios in an initially homogeneous magma might change during eruption and emplacement of an ash-flow tuff. Perhaps, comminution during eruption or flow preferentially 'destroys' some phases and preserves others (i.e., makes grains so small that they appear to be part of the matrix or are blown out of the tuff during flow). If this hypothesis is invoked to explain mineral proportions seen in the Lund Tuff, then quartz and sanidine whose proportions increase must be resistant to fragmentation and plagioclase, hornblende, and Fe–Ti oxides would fragment easily and be obliterated. We see no reason why quartz and sanidine would be more resistant to comminution than opaques or plagioclase. Moreover, the comminution hypothesis predicts that quartz and sanidine *abundance* would change little and other phases would decline in abundance to elevate the quartz/plagioclase ratio. This is contrary to

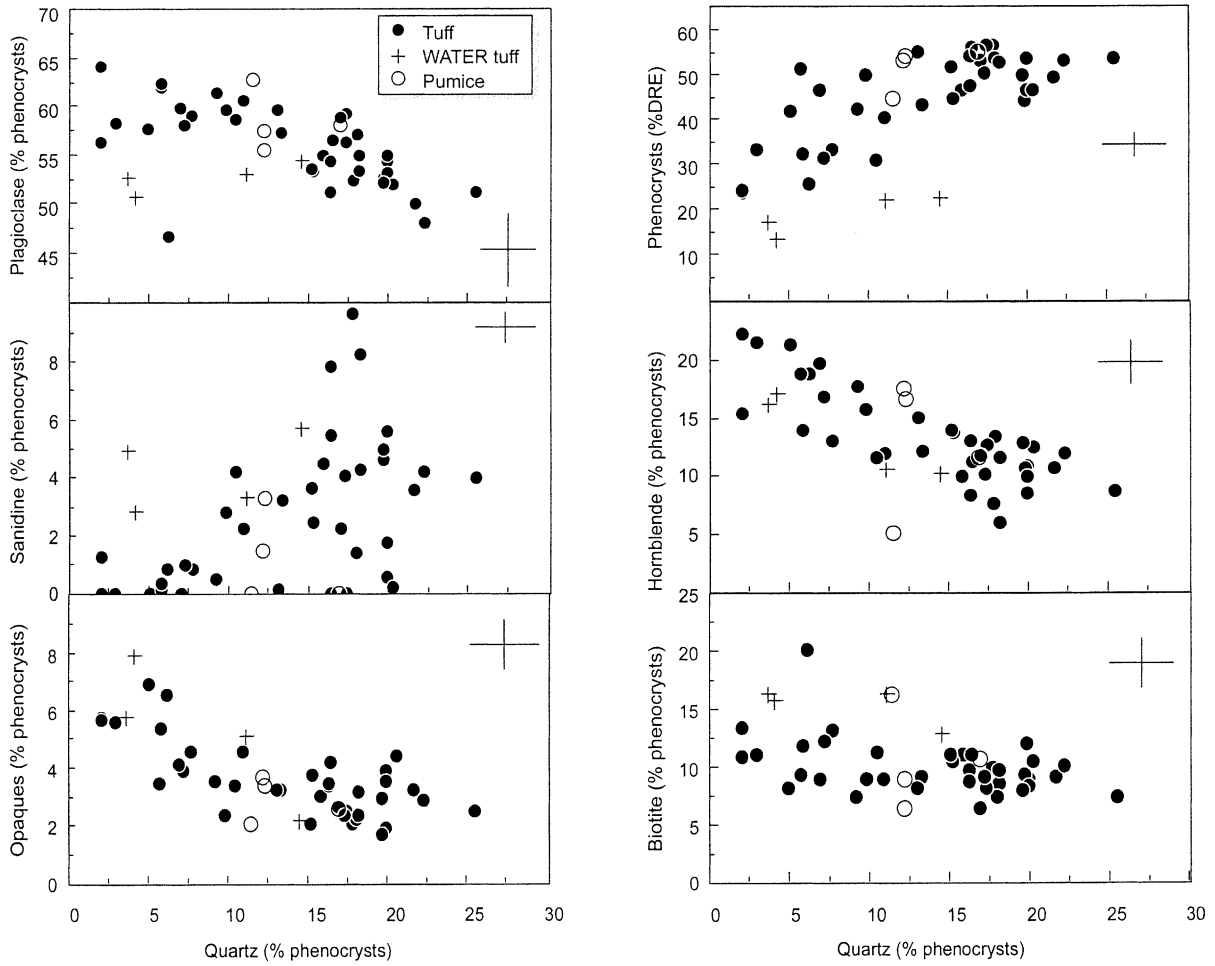

Fig. 5. Modal proportions of phenocrysts (as % of total phenocrysts) in Lund Tuff. Error bars represent maximum range in modes of replicate thin sections of same sample at indicated modal %.

our observations; quartz abundance (corrected to dense rock) varies and plagioclase abundance is less variable. In other words, the quartz/plagioclase ratio decreases because of increasing quartz, none of which appears to be restitic or xenocrystic. Finally, Best and Christiansen (1997) showed that *phenoclasts* in large-volume ash flows are not significantly affected by abrasion during flow and instead are fragmented by explosive expansion of melt inclusions. Consequently, we conclude that the changes in mineral proportion are not the result of emplacement processes, but reflect different mineral proportions in the parental magma. In fact, these modal trends (increasing proportions of quartz and sanidine with declining proportions of mafic phases) are consistent with the normal evolution of a crystallizing silicic magma.

In our small suite of pumice samples, phenocryst proportions do not vary as much as in the tuff, but they fall within the range for the tuff (Figs. 4 and 5).

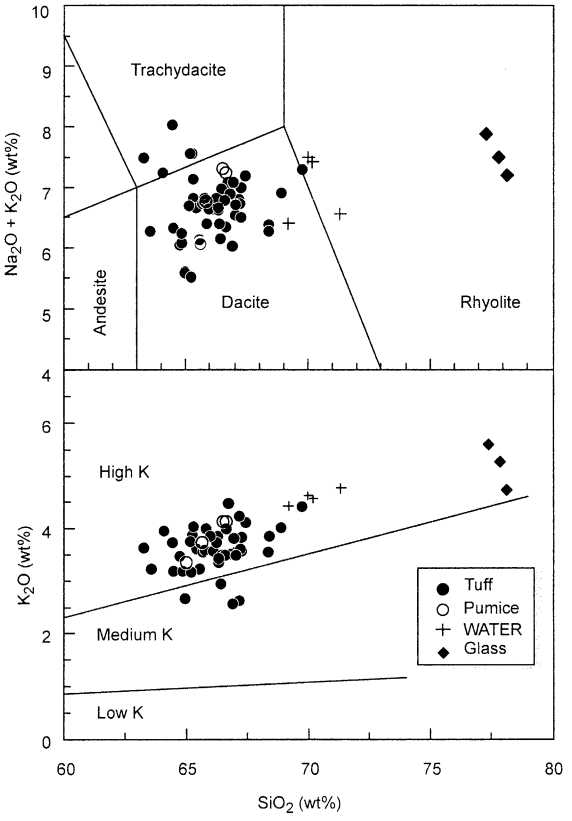

Fig. 6. IUGS chemical classification (LeMaitre, 1989) of Lund Tuff. Oxide percentages normalized to 100% volatile-free.

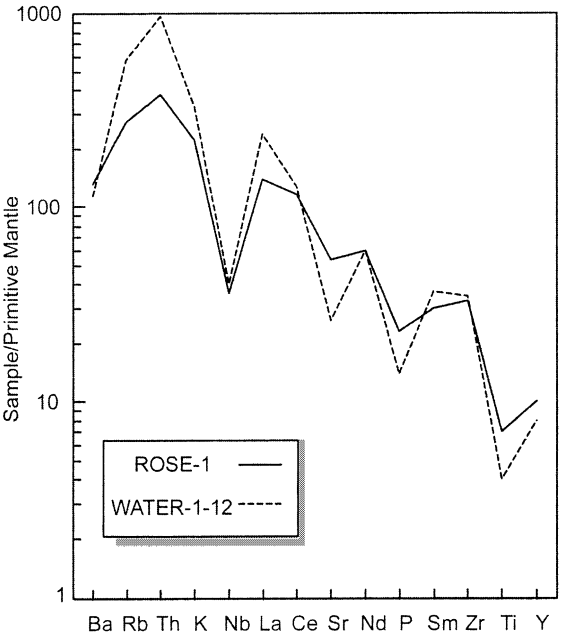

Fig. 7. Normalized (McDonough and Sun, 1995) trace element diagrams of representative Lund Tuff samples. The most evolved sample is WATER-1-12 and the least evolved is ROSE-1.

4.2. Whole-rock chemical composition

Most samples of Lund Tuff (Table 3; Fig. 6; Appendix B[3]) are dacites but post-eruption mobility of alkalies probably displaced some into the trachydacite field. Two samples in the phenocryst-poor Y (WATER) section are low-silica rhyolites. The Lund Tuff is calc-alkaline, based on low Fe/(Fe+Mg) ratios, and is high-K. Normalized trace element patterns (McDonough and Sun, 1995) show negative Ba, Nb, Sr, P, and Ti anomalies and decreasing enrichment of the more compatible elements (Fig. 7). Negative Nb and Ti anomalies indicate a subduction-related magma, or one containing components from preexisting continen-

[3] See Electronic Supplements on http://www.elsevier.com/locate/jvolgeores

tal crust. The depletion in Ba may reflect removal of biotite. The Sr, P, and Ti anomalies are slightly more pronounced in the most silicic samples, suggesting that separation of plagioclase, apatite, and Fe–Ti oxides affected them. The Lund Tuff compositions also lie in the volcanic arc-granite field of Pearce et al. (1984) on the discriminant plot of Rb vs. Y+Nb.

The range of major element variations in the Lund Tuff (Figs. 6 and 8) is comparable to those in many systematically zoned tuff deposits. Although virtually all of the Lund samples are dacite, the range in silica (about 8% on an anhydrous basis) is no less than that of many deposits zoned from rhyolite to dacite. However, strongly compatible elements in the Lund Tuff vary by relatively small factors (Mg, 2.7; Sr and P, 1.7) whereas in the zoned Pahranagat Tuff (Best et al., 1995) these elements vary by factors of 5–7 and in the Bishop Tuff by factors of about 10 (Hildreth, 1979).

An apparent paradox is that variations in

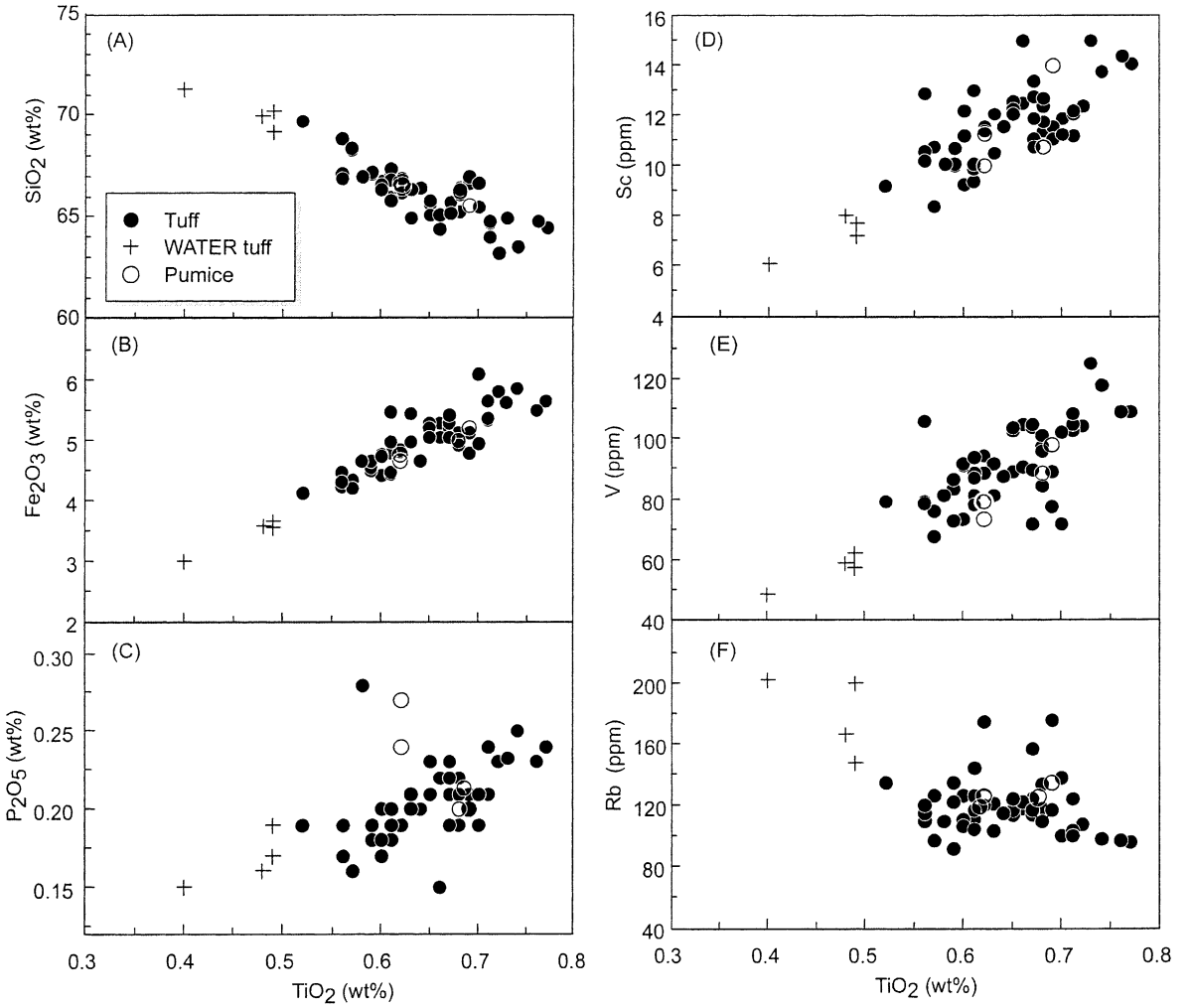

Fig. 8. Selected whole-rock major and trace element compositions plotted against TiO_2 for the Lund Tuff. Major element oxides are normalized to 100% volatile-free.

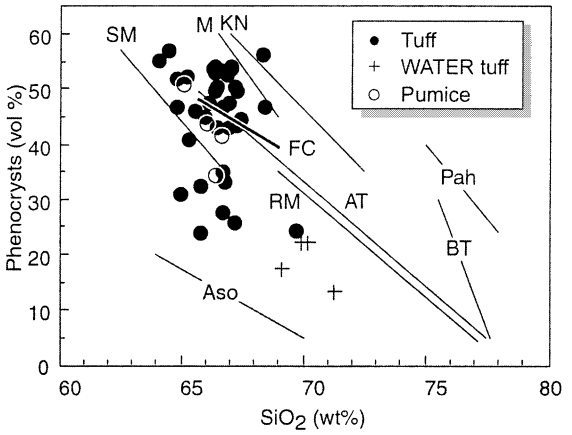

Fig. 9. Whole-rock SiO_2 versus total abundance of phenocrysts, adjusted to dense rock equivalent, in the Lund Tuff compared with the Pahranagat Tuff (Pah; Best et al., 1995) and selected other tuff deposits from Hildreth (1981) as follows: BT, Bishop Tuff; AT, Ammonia Tanks; RM, Ranier Mesa; FC, Fish Canyon; KN, Kneeling Nun; M, Monotony; SM, Snowshoe Mountain.

whole-rock chemical and modal compositions correlate only weakly and not at all if the glass-rich WATER samples are ignored (Figs. 9 and 10).

4.3. Vertical and lateral compositional variations

Stratigraphic sections were sampled to test for vertical compositional variations in the Lund deposit. These include outflow sections A on the east and U on the west, intracaldera section C, and older caldera fill section S on the east (Fig. 2). Representative modal and chemical data for these sections are shown in Fig. 11. There is no systematic vertical variation in ratios of phenocrysts in the Lund deposit. On the other hand, in all but the western outflow section, there is a subtle and inconsistent reverse zonation shown by decreasing MgO and TiO_2 and increasing K_2O. This may reflect a small upward decrease of about 10% in the crystal/glass ratio in two of the sections.

With regard to lateral variation, the average elemental composition of the outflow tuff is indistinguishable from the intracaldera tuffs. For example, average SiO_2 (66.4% ± 1.9 versus 66.4% ± 1.0) and TiO_2 (0.64% ± 0.8 versus 0.63% ± 0.06) are practically identical in the outflow tuff and intracaldera tuff respectively. Likewise, we have not detected any sectoral differences in the elemental composition of the outflow sheet. On the other hand, there are significantly fewer phenocrysts (on a dense rock basis) in the outflow than in the intracaldera tuffs (33.8 ± 11.9% versus 50.6 ± 4.0%). The significance of this difference is compromised somewhat by the correction to dense rock equivalent percentages, but seems to be outside of the 10% error in our density corrections. In terms of phenocryst proportions, quartz is lower (8.9% ± 5.2 versus 16.9% ± 4.5) and total mafics higher (32.2% ± 7.0 versus 24.9% ± 3.4) in the outflow compared to the intracaldera tuff. This is another example of the apparent decoupling of elemental composition from phenocryst proportions.

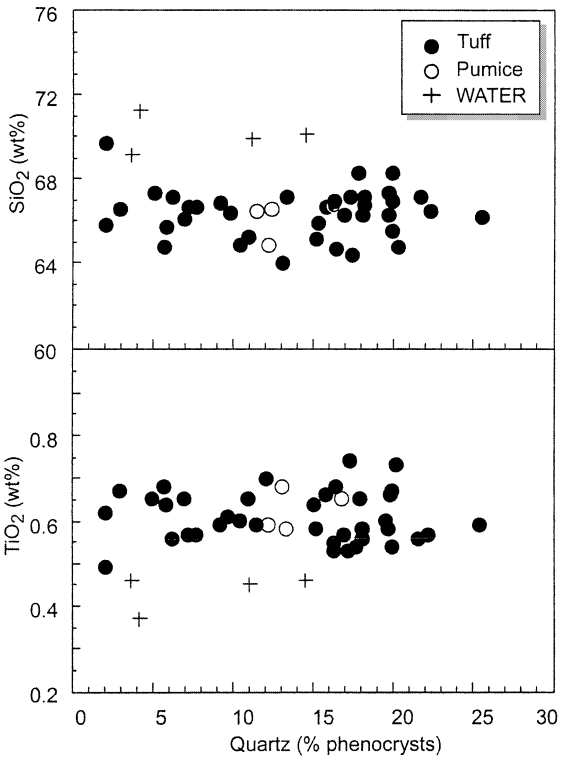

Fig. 10. Whole-rock SiO_2 and TiO_2 versus modal proportion of quartz in the Lund Tuff. Note the lack of chemical variation with respect to modal quartz. Other elements, such as Fe_2O_3, MgO, Sc, and V, also show no covariation with modal quartz. Three samples from the WATER (Y) section have lower TiO_2 and higher SiO_2 as a result of glass enrichment.

5. Chemical composition of phases

Phenocrysts and glass were analyzed by electron microprobe in seven Lund Tuff samples. Silicate and ilmenite phenocrysts are unaltered and gave acceptable analytical totals. Magnetite grains are slightly oxidized along fractures and rims but unaltered interiors were analyzed. The only obvious zoning in mineral grains occurs in plagioclases; different mafic grains within a sample are somewhat variable in composition but unzoned. Representative analytical data are in Table 4.

Plagioclase is zoned andesine, about An_{35} to An_{50}; disregarding possible restite cores of labradorite found in one sample. Sanidine varies between Or_{84} and Or_{74} and was not found in the most mafic (high-TiO_2) samples. Compositions of biotites and amphiboles, which are almost all low-Al magnesiohornblendes, vary significantly and do not correlate strongly with host rock chemical composition (Fig. 12). However, Mg-rich and Mn-poor phenocrysts occur in the more mafic samples. Magnetites have a small but significant range in composition as well and are rich in Mg and Al in the more mafic samples. Variations in ilmenite are limited. The high Mg/Fe ratios in biotite and hornblende found in the low-TiO_2 WATER samples show the rocks are not rhyolitic differentiates of the Lund magma, but instead mechanical mixtures enriched in TiO_2-poor (and silica-rich) glass and depleted in phenocrysts (Fig. 12).

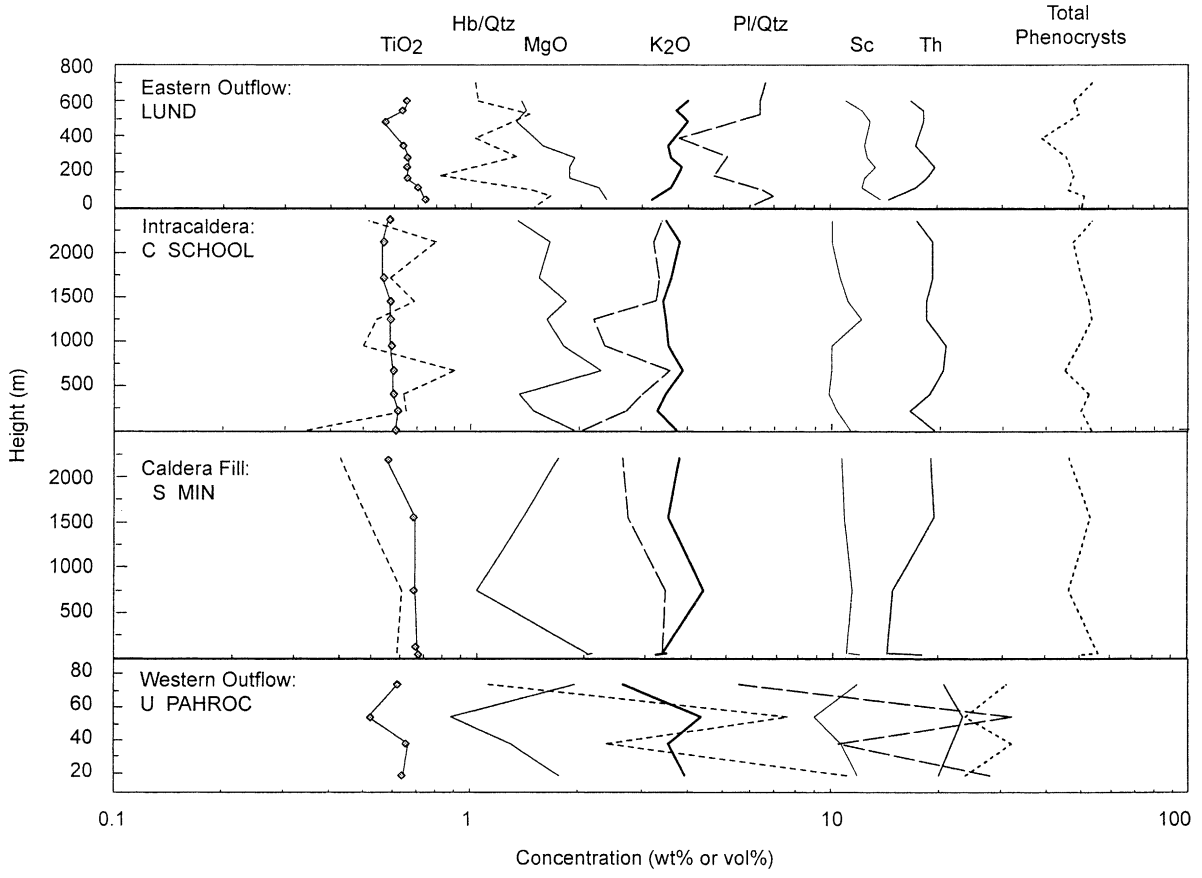

Fig. 11. Representative modal (dashed lines) and chemical (solid lines) data for stratigraphic sections in the Lund Tuff (Fig. 2). Logarithmic scales are used to display the wide range of concentrations and to allow direct comparison of percent of vertical change. Intracaldera section lies within its own White Rock caldera; caldera-fill section lies within older unrelated Indian Peak caldera.

Table 4
Representative electron microprobe analyses of minerals in the Lund Tuff[1]

	Sanidine	Plagioclase		Biotite		Hornblende		Magnetite		Ilmenite	
	COYOT 1E	PAHRC 2C	COYOT 1E	PAHRC 2C	COYOT 1E	PAHRC 2C	COYOT 1E	PAHRC 2C	COYOT 1E	PAHRC 2C	COYOT 1E
SiO_2	63.74	58.24	58.55	37.54	37.23	46.20	46.38	0.03	0.04	0.02	0.03
TiO_2				4.73	4.24	1.57	1.39	5.43	4.73	35.22	36.18
Al_2O_3	19.18	26.27	26.39	13.55	13.53	8.18	7.83	1.75	1.47	0.20	0.10
V_2O_3								0.61	0.53	1.51	1.42
Cr_2O_3								0.06	0.06	0.03	0.01
FeO_t	0.13	0.27	0.25	16.14	16.93	14.13	14.73				
Fe_2O_3*								54.96	57.99	32.28	30.72
FeO*								33.54	34.33	28.51	29.94
MnO				0.21	0.29	0.48	0.50	0.73	0.49	0.77	0.53
MgO				14.12	13.90	13.56	13.52	1.03	0.67	1.35	1.17
CaO	0.15	8.50	8.09	0.01	0.01	11.33	11.41				
Na_2O	2.73	6.36	6.58	0.48	0.46	1.46	1.41				
K_2O	12.07	0.65	0.66	9.03	9.06	0.91	0.89				
BaO	0.95	0.06	0.04								
F				0.51	0.57	0.30	0.27				0.38
Cl				0.14	0.13	0.09	0.11				
H_2O*				3.65	3.61	1.89	1.91				
Total	98.95	100.34	100.56	99.86	99.69	99.97	100.20	99.15	100.31	99.91	100.10

Average analyses in weight percent, used in intensive variable calculations. H_2O* calculated from cation normalized formulas assuming full occupancy of the hydroxyl site in biotite and hornblende. FeO* and Fe_2O_3* calculated using method of Ghiorso and Sack (1991).

[1] For other electron microprobe analyses are given in Appendix C; see Electronic Supplements on http://www.elsevier.com/locate/jvolgeores

The ranges of chemical variation in phenocrysts in the Lund Tuff are comparable to those in systematically zoned deposits (Fig. 13), such as the Bishop Tuff (Hildreth, 1979) and Pahranagat Tuff (Best et al., 1995) indicating that there was significant variability in the parental magma chamber before eruption, despite the apparent absence of systematic zoning.

Even though electron microprobe analyses reveal perturbed alkali concentrations, glass in the Lund Tuff is a high-silica, low-Ti–Fe–Mg–Ca rhyolite.

6. Intensive parameters in Lund magma

Calculations of intensive parameters from mineral compositions in bulk tuff samples are complicated by phenocryst mixing that may occur during eruption. However, within individual samples grain to grain composition differences are not great compared to the total compositional range (Maughan, 1996). Consequently, we used average compositions for the unzoned mafic phases and sodic rims of zoned plagioclase grains (to get minimum temperature estimates). In addition, Fe–Ti oxide temperatures were calculated only from magnetite and ilmenite grains that passed a test for equilibrium (Bacon and Hirschmann, 1988). The highest temperatures were found for the more mafic rocks, with the exception of the WATER samples (Table 5). Calculated temperature and oxygen fugacities follow a trend two to three log units above QFM. This is the same fO_2 trend as other silicic igneous rocks that contain titanite, magnetite, and quartz (Wones, 1989). Temperatures derived from hornblende–plagioclase (Holland and Blundy, 1994), biotite (Luhr et al., 1984), and two feldspar geothermometers (Fuhrman and Lindsley, 1988) are generally similar. Pressures, calculated from the Al-in-hornblende calibration of Johnson and Rutherford (1989a), cluster at about 2.5 kb (Fig. 14).

The inferred fO_2, temperature, and pressure of

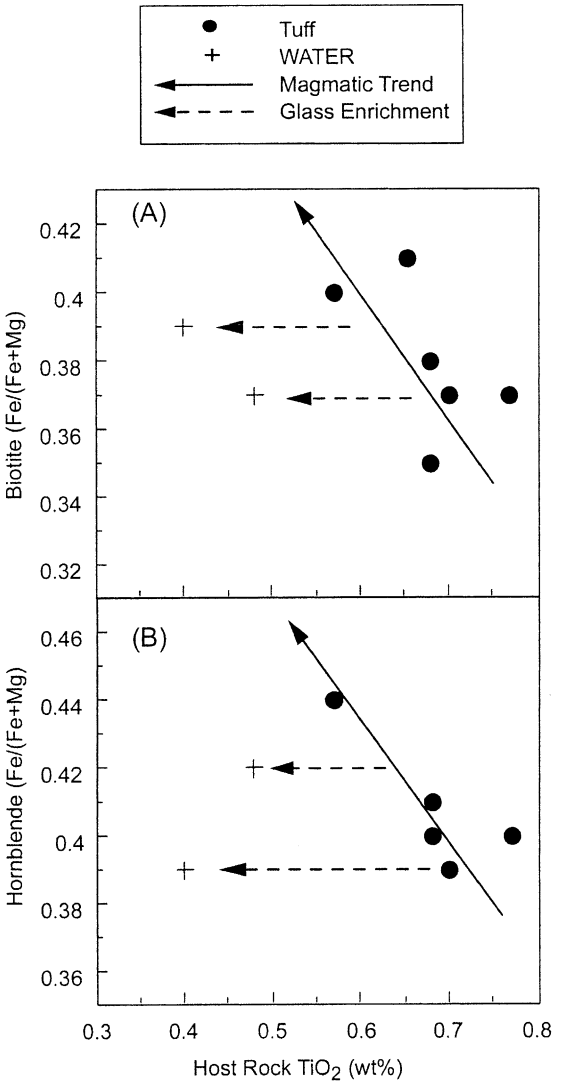

Fig. 12. Fe/(Fe+Mg) in (A) biotites and (B) hornblendes versus whole-rock TiO_2 concentrations in host-rock Lund Tuff. Two samples (WATER-12M and -34M from site Y) with low TiO_2 concentrations are believed to have been displaced (dashed line) off the main compositional trend (solid line) because of enrichment of host rock in low-TiO_2 glass (see Fig. 15).

crystallization and the phenocryst assemblage of the Lund Tuff agree with the Fish Canyon phase equilibria determined experimentally by Johnson and Rutherford (1989b). Of samples plotted in Fig. 14, only the high-temperature samples PAHRC-2C, LAM-5V, and ROSE-1 lack sani-

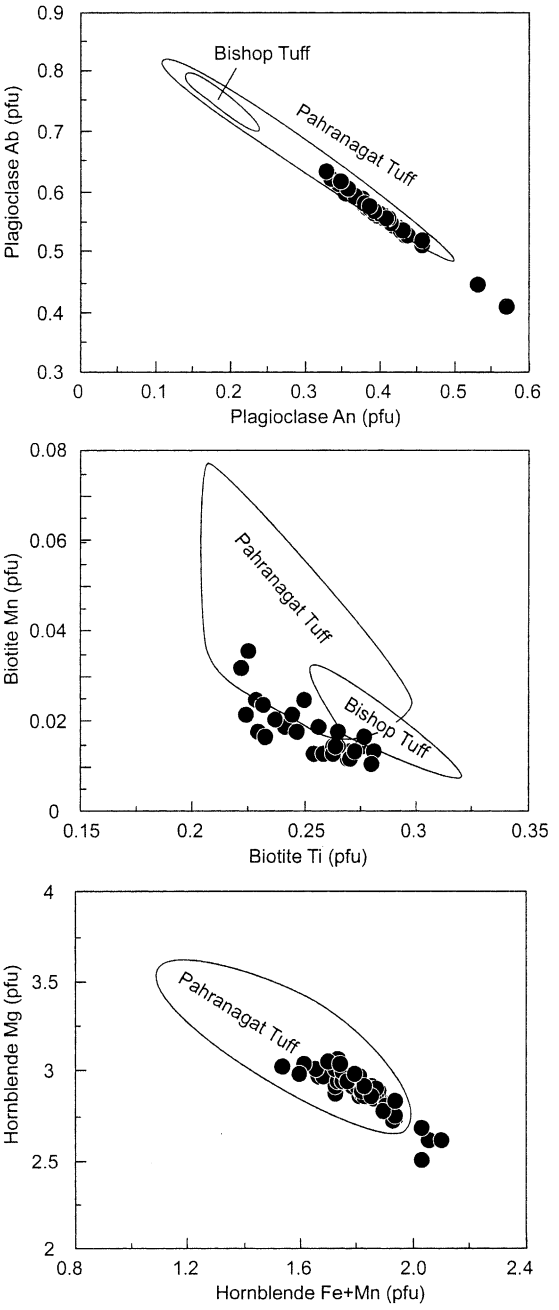

Fig. 13. Compositions of Lund phenocrysts (filled circles; pfu, per formula unit) compared to those in systematically zoned rhyolite tuff deposits. Bishop Tuff (Hildreth, 1979). Pahranagat Tuff (Best et al., 1995).

dine whereas the other samples contain phenocrysts of sanidine+quartz+plagioclase+biotite+hornblende+Fe–Ti oxides+titanite. A few Lund samples contain trace amounts of clinopyroxene partially reacted to hornblende that might be relicts of higher temperatures of crystallization. In short, the Lund Tuff magma appears to have crystallized at modest depth (about 8 km) under oxidizing but water-undersaturated ($X_{H2O} = 0.5$) conditions. However, pre-eruption temperatures in the tuff were not homogeneous and ranged from about 740°C to 800°C. Different equilibration temperatures could have caused the varying phase proportions and presence or absence of sanidine.

7. Implications of the composition of the Lund Tuff

7.1. Summary of facts

Nearly all samples of the Lund Tuff contain the same phenocryst assemblage; in this regard the Lund Tuff is monotonous. Only in mafic samples, with high equilibration temperatures and high TiO_2, is sanidine absent. Phenocryst ratios vary by as much as an order of magnitude in a manner consistent with progressive crystallization of cooling silicic magma. Element concentrations vary by as much as a factor of two or three along normal differentiation trends for calc-alkaline magmas. Major element composition is only weakly corre-

Table 5
Intensive parameters calculated for the Lund Tuff magma

Sample	PAHRC-2C	LAM-5V	COYOT-1E	HOR-11	WATER-1-12M	ROSE-1	WATER-1-34M
Temperature (°C)							
Two-feldspar							
Fuhrman and Lindsley (1988)			770	745			
Biotite							
Luhr et al. (1984)	815 ± 2	805 ± 29	765 ± 32	731 ± 21	818 ± 22	800 ± 17	765 ± 29
Hornblende–plagioclase							
Holland and Blundy (1994)	762 ± 22	755 ± 21	784	755 ± 6			772 ± 8
Fe–Ti oxides							
Ghiorso and Sack (1991)	860 ± 5		802 ± 12	708			
Preferred temperature	788	765	773	735	818	800	765
Pressure (kb)							
Hornblende							
Johnson and Rutherford (1989a)	2.5 ± 0.3	2.6 ± 1.4	2.2	2.5 ± 0.4	2.9 ± 0.5	2.5 ± 0.2	2.5 ± 0.3
Anderson and Smith (1995)	1.9 ± 0.3	2.8 ± 0.4	2.0	2.9 ± 0.4	1.5 ± 0.5	2.0 ± 0.2	2.4 ± 0.3
Oxygen fugacity							
Fe–Ti oxides							
Ghiorso and Sack (1991)							
$\log f O_2$	−10.7		−11.7	−14.1			
ΔQFM	2.7		2.8	2.7			
Water fugacity (kb)							
Biotite–magnetite–sanidine							
Bohlen et al. (1980)	2.7 ± 0.2		3.1 ± 0.3	2.1 ± 0.4			

Hornblende pressures and water fugacities calculated using preferred temperature.

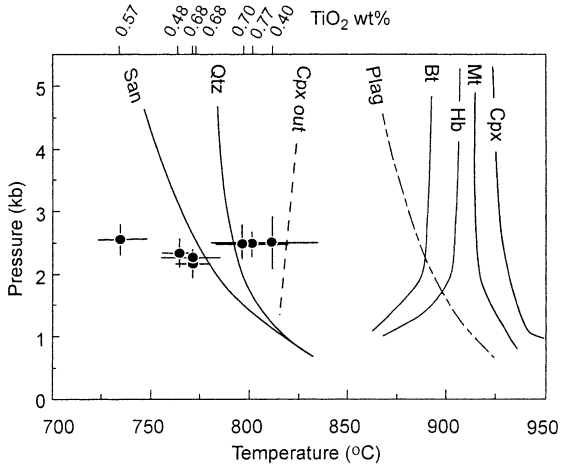

Fig. 14. *P–T* diagram comparing preferred eruption temperatures and average pressures for Lund Tuff to mineral stability fields for the Fish Canyon magma system at $X_{H2O} = 0.5$ (Johnson and Rutherford, 1989b). Solid curves represent the beginning of crystallization with decreasing *T* of indicated crystalline phases. Dashed line labeled 'Cpx out' represents the low-*T* stability limit of clinopyroxene as it reacts with melt to produce hornblende. Crosses for each sample are ±1 standard deviation (Table 5).

lated ($r^2 \approx 0.5$) with proportions of plagioclase, hornblende, opaques, and total phenocrysts (Fig. 10). Mineral compositions are not strongly correlated with whole-rock chemical composition (if the glass-rich WATER samples are included, Fig. 12). Matrix glass in the Lund Tuff is high-silica rhyolite. The Lund deposit lacks systematic vertical variations in modal composition but a weak reverse zonation is evident in some elements in some sections that may reflect a slight upward increase in the proportion of glass to phenocrysts. The absence of a plinian fallout tuff and of a rhyolitic base beneath the voluminous crystal-rich dacite tuff are especially significant.

The Lund deposit, therefore, appears monotonous in some respects but has variations in modal, mineralogical, and bulk chemical composition.

7.2. Anomalous WATER samples at site Y

The samples from the western Y section are anomalous in several respects. That they are truly from the Lund Tuff cannot be doubted because WATER-22M has a Lund age (Table 2) and mineral compositions are like those in the rest of the tuff. Relative to other Lund samples, they have extreme major and trace element compositions, such as low TiO_2, Fe_2O_3, Sc, and V and high silica (Figs. 6, 8 and 15) and include the only low-silica rhyolites analyzed. They are also phenocryst-poor (Fig. 9), to as little as 10% of the whole rock (about 13% on a dense rock basis), and the phenocrysts are uniformly smaller. These rhyolites are not simply silicic differentiates of the main dacitic part of the magma chamber because their biotite and hornblende phenocrysts have low Fe/(Fe+Mg) ratios and yield high equilibration temperatures just like the dacites (Fig. 12; Table 5).

However, their attributes are consistent with enrichment in high-silica rhyolite vitroclasts (Fig. 9). As apparent in Fig. 15, 1.4 times as much glass must be added to a Lund Tuff that has 0.76 wt% TiO_2 to create the WATER-12M sample that contains 0.40 wt% TiO_2. This added glass would convert an average Lund Tuff containing 40% phenocrysts into one that has the same phenocryst content as WATER-12M.

7.3. Discussion

The conclusion of Whitney and Stormer (1985) that the compositional variability of the Fish Canyon Tuff was created by different degrees of winnowing of vitroclasts from an initially homogeneous magma during explosive eruption and emplacement cannot apply to the Lund Tuff. From major element plots (Figs. 8 and 15), it might be concluded that whole-rock chemical variations in the Lund Tuff simply resulted from differential winnowing of glass from phenocrysts. However, it is inconceivable that any elutriation process could have created these features from a homogeneous magma. Four lines of evidence support this contention: (1) order-of-magnitude variations exist in ratios of phenocrysts; (2) there are systematic modal variations; (3) the phenocrysts are chemically variable; and (4) there is a significant range of inferred crystallization temperatures. Elutriation of glass would have created a marked correlation between whole-rock chemical composition and total abundance of phenocrysts,

but any such correlation for the Lund Tuff is weak and, if the silicic WATER samples – which cannot be regarded as parental glass-rich magma – are disregarded the correlation is nonexistent (Fig. 9). The absence of significant phenocryst enrichment is also illustrated by the high phenocryst proportions in the cognate inclusions when corrected to a dense rock basis. In fact, they are on average slightly enriched in phenocrysts ($52 \pm 4\%$ versus $43 \pm 12\%$). Glass elutriation would create the opposite trend. The conclusion seems inescapable that the erupted, very large volume Lund magma was inhomogeneous with regard to proportions and ratios of phenocrysts, mineral compositions, and equilibration temperatures.

We next examine the possibility that some of the variability in bulk composition and in phenocryst ratios and compositions represent differing degrees of crystallization at different values of intensive parameters, especially temperature. We have already noted that the trends of variations in phenocryst proportions are consistent with progressive crystallization of a dacitic magma. Yet, on the other hand, Figs. 9 and 10 show a weak correlation between bulk rock composition and phenocryst compositions. There is also little correlation between phenocryst abundance and elemental composition. A 2–25% variation in the proportion of quartz phenocrysts to total phenocrysts does not correspond with any significant variation in any chemical constituent, not even silica.

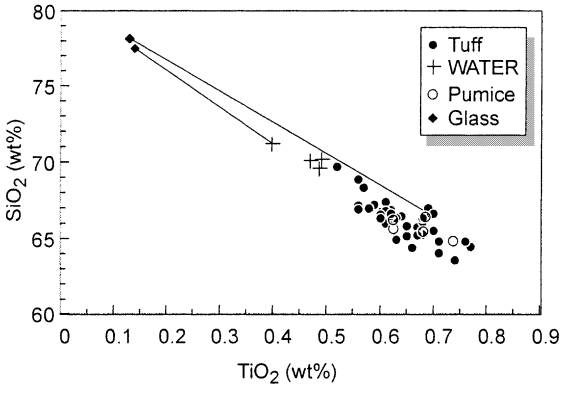

Fig. 15. Compositions of glass in Lund Tuff connected by tie-lines to their corresponding whole-rock hosts. WATER-1-12, -22, and -34 whole-rock samples (+) lie at the extremity of the tuff field because of enrichment in low-TiO_2 glass.

What then caused the range of compositions? Fractional crystallization of mafic dacite was tested by Maughan (1996) using the major element fractional crystallization program of Stormer and Nicholls (1978) and found to be an unsatisfactory solution to the whole-rock chemical variation – as expected for a phenocryst-rich rock treated as a liquid.

Trace element models (Fig. 16) can also be used to test this and other evolutionary hypotheses. Bulk partition coefficients were calculated from the average modal proportions and partition coefficients from Rollinson (1993). The relatively small variations in compatible element concentrations (like Sr) are inconsistent with simple fractional crystallization (Fig. 16A). Nor are the trace element trends consistent with combined fractional crystallization and mixing of melts (pyroclasts) during eruption (cf. Best et al., 1995). The only pyroclast mixing trends (Fig. 16B) that satisfy the bulk of data involve highly fractionated melts ($F < 0.2$, where F is the fraction of residual liquid) mixing with rather primitive melts ($F > 0.9$). Mixtures involving intermediate compositions along the fractionation trend are not apparent but should be much more common than mixtures of the extremes. We have no evidence of the existence of contrasting liquids – all of the analyzed glasses are fairly homogeneous rhyolitic glasses. In addition, modeling a phenocryst-rich magma as an evolving liquid seems inappropriate.

Batch partial melting followed by accumulation of different batches of magma in a sub-caldera chamber might explain the observed trace element trends (Fig. 16C). Here we have assumed partition coefficients appropriate for a broadly dacitic melt – rather high D_{Sr} (3) because of abundant plagioclase and low D_{Rb} (0.1) to represent little or no biotite in the residuum. Liquid compositions produced by partial melting crust of broadly andesitic composition ($C_o^{Rb} = 70$ ppm, $C_o^{Sr} = 900$ ppm) correspond rather closely with the Lund Tuff. However, such models require very high degrees of melting, ranging as high as 0.8. To match the magma composition by using lower degrees of

melting, the source must have unrealistically high Sr contents ($Sr_o = 1300–1400$ ppm; $Rb_o = 35$). In any case, it is difficult to see how separate batches of magma could be inserted sequentially in a shallow magma chamber without thorough mixing or systematic zoning. In addition, these partial melting models do not directly address the high crystallinity of the rocks, since the models are for melts only.

Several open system models must also be considered as possible explanations for the trace element data. For example, the composition of the Lund Tuff lies on potential mixing trends between some andesites and rhyolites (Fig. 16D) that erupted both before and after the tuff (Best and Christiansen, 1989a). However, if magma mixing occurred, homogenization was extensive as phenocrysts with compositions similar to those found in the andesites are absent (calcic plagioclase cores have inclusions of biotite and are unlikely to have crystallized from Indian Peak andesites that generally contain two-pyroxenes or olivine). Nor are disequilibrium textures the rule in the Lund Tuff. Again, this model provides no explanation for the phenocryst-rich magma. Mixing would have to have been followed by re-equilibration and considerable crystallization.

Another relatively unsuccessful set of open-system models involves assimilation combined with fractional crystallization (Fig. 16E). Two end-member models are shown. One involves assimilation of average upper continental crust (Taylor and McLennan, 1985). Even over a wide range of possible contamination/assimilation ratios ($r = 0.3$ for the model shown) these models do not match the trends seen in the tuff. A closer match can be made by assuming that a highly evolved rhyolite was mixed into a fractionating dacitic magma. However, the composition of assimilated rhyolite must be rather extreme (at $r = 0.3$; 1000 ppm Rb and 50 ppm Sr-like a topaz rhyolite; Christiansen et al., 1983). At higher rates of assimilation/crystallization ($r = 0.95$), the hypothetical rhyolite contaminant is less unusual but still 400 ppm Rb is required to match the shallow trend of the Lund Tuff. However, Rb-rich topaz rhyolite lava flows in the area post-date the Lund Tuff by at least 6 Myr. Open system models like this also predict a large range in isotopic compositions of the mafic versus the more silicic rocks. Isotopic data collected thus far do not demand large amounts of open system addition of extraneous components – solids or liquids – to the Lund magma system. $\delta^{18}O$ for quartz in mafic versus more silicic Lund Tuff varies by 1‰ and for plagioclase shows no discernible differences (Hart, 1997). Likewise, Pb–Sr–Nd isotope ratios (Hart et al., 1998) show very little isotopic variation across

Fig. 16. Petrogenetic models for the compositional variation in the Lund Tuff. (A) Rubidium and strontium variations in the Lund Tuff compared to the evolution of a magma experiencing fractional crystallization (line labeled by fraction of residual liquid – F). Bulk partition coefficients ($D_{Rb} = 0.25$, $D_{Sr} = 3.8$) were calculated from the modal mineralogy and initial concentrations were taken from the most mafic rock composition ($C_o^{Rb} = 95$ ppm, $C_o^{Sr} = 650$ ppm), but the conclusions are not sensitive to a rather wide range of assumptions. (B) The thin lines illustrate only a few of the many mixing lines between melts produced by varying degrees (F) of fractional crystallization. Mixtures close to the fractionation line would be expected to be abundant but are not apparent in the Lund Tuff. (C) Melts produced by variable degrees of batch partial melting (shown with line labeled with fraction of melting) correspond to the compositional variation of the Lund tuff. A crustal source with $C_o^{Rb} = 70$ ppm. $C_o^{Sr} = 900$ ppm was assumed. (D) The Lund Tuff lies on nearly straight-line mixing trends between some of the andesites and rhyolites that erupted before and after (30–25 Ma) the Lund Tuff. (Includes unpublished data from the Indian Peak Volcanic Field collected by M.G. Best and E.H. Christiansen). (E) The effect of assimilation and fractional crystallization on rubidium and strontium concentrations (lines labeled with F – fraction of residual liquid) as compared to the Lund Tuff. The ratio of the rate of assimilation to crystallization is r and assumed to be 0.3. Assimilation of upper continental crust (Rb = 112, Sr = 350; Taylor and McLennan, 1985) does little to perturb the fractional crystallization curve. However, hypothetical evolutionary trends can be found that fall near the bulk rock compositions by assuming assimilation of highly evolved rhyolite (Rb = 1300 ppm, Sr = 50 ppm). Bulk partition coefficients ($D_{Rb} = 0.25$, $D_{Sr} = 3.8$) and initial composition of melt ($C_o^{Rb} = 95$ ppm, $C_o^{Sr} = 650$ ppm) are the same as those in model A. (F) Equilibrium crystallization with the production of coexisting crystals and liquids (solid curves labeled with F – the fraction of residual liquid). The dots are the compositions of 50/50 mixtures of crystals and melts produced by mixing at each 10% crystallization increment. Mixing may have occurred during eruption. The tuff compositions correspond to the most common set of these mixtures.

the compositional spectrum in the Lund Tuff. Therefore, open system models are not very attractive explanations for the variation in the tuff. These models also suffer because they treat the evolving magma as a crystal-free melt.

These model calculations do not preclude batch partial melting, magma mixing, or assimilation as important processes in the *generation* of the Lund magma; the models simply show that these processes were not responsible for the observed *chem-*

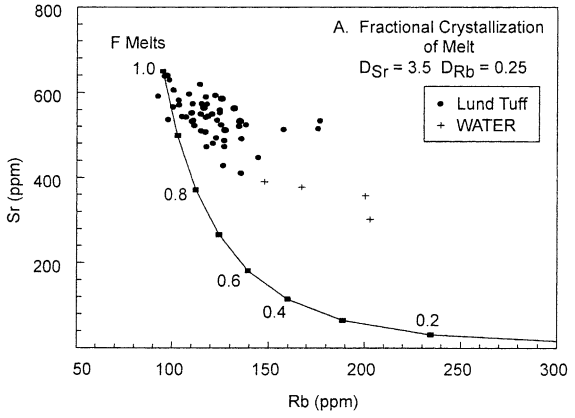

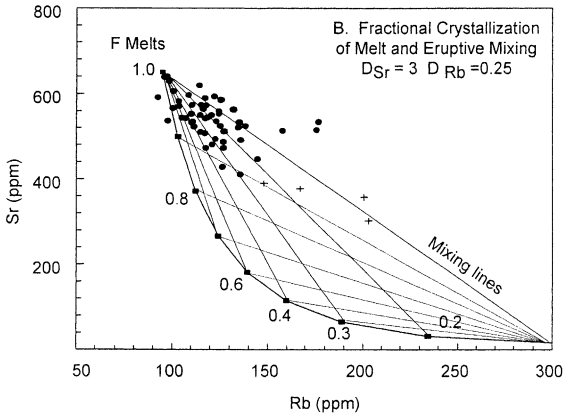

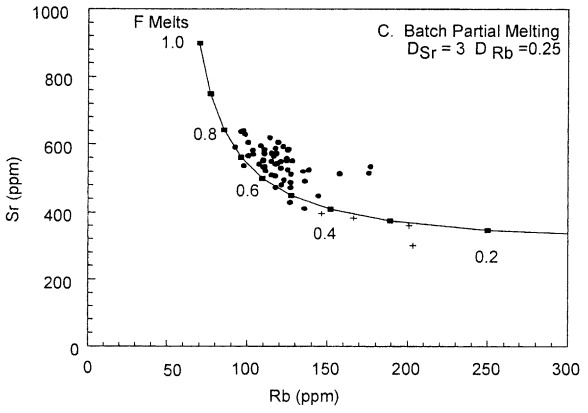

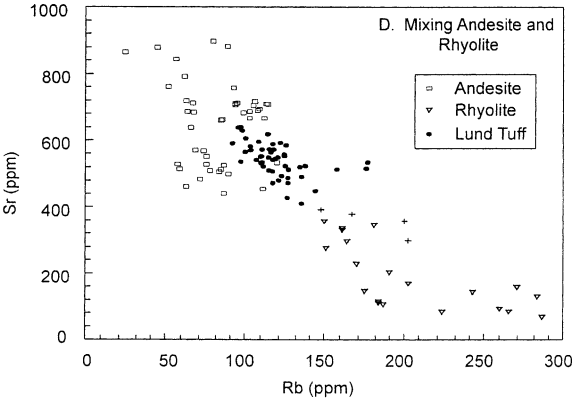

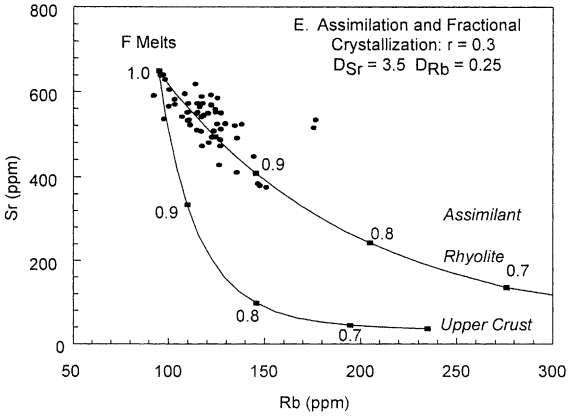

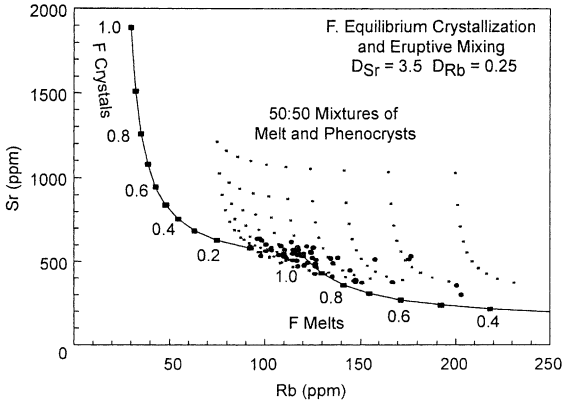

ical variation in the tuff. In fact, it is our contention that the chemical evidence is consistent with the generation of the Lund parental magma by interaction of mafic magmas with more silicic crust and magmas derived from it.

More successful models of the trace element and phenocryst variations of the Lund Tuff can be created by assuming that varying degrees of fractional crystallization (+/−some small amount of assimilation or mixing) of a parental magma produced a range of complementary melts and crystals that coexisted in the same chamber. If these components were then separated and remixed during explosive eruption, they would produce a shallow trend on a Rb–Sr diagram. However, for the assumptions used here, the models predicts that the bulk tuff samples should consistently have $>50\%$ phenocrysts, when in fact few of our samples do. Choosing a more Rb-rich parent as the initial melt only makes this problem worse; assuming an initial magma with less Rb is unable to explain the high Rb rocks.

The most successful closed system models involve *equilibrium crystallization*, rather than fractional crystallization. Equilibrium crystallization may be a better model for a large convecting magma system such as the one that must have fed the Lund Tuff. The range of phenocryst proportions, phenocryst compositions, and inferred temperatures implies that the degree of evolution varied in different parts of the parental magma chamber. Thus, 'discrete parcels' of melt and crystals may have coexisted in a thermally inhomogeneous, convecting magma chamber. Each parcel would have had a different degree of crystallinity. On this diagram (Fig. 16F), the bulk tuff compositions are enclosed by a field of hypothetical 50:50 mixtures (small dots) of melts and coexisting solids produced at 10% increments of crystallization. Physical mixing could have occurred during eruption of vitroclasts and phenoclasts. Glass from one parcel could mix with crystals from another parcel and produce a wide range of phenocryst proportions and bulk rock compositions. The compositions of the tuff samples fall within the densest cluster of mixtures.

This, our preferred model, explains many aspects about the Lund Tuff: (1) the compositional variation in the tuff but the absence of systematic zonation in the deposit; (2) the crystal-rich character of the pumices and of the tuff, (3) the relatively flat Rb–Sr trends (and for other elements not shown here for lack of space), (4) the varying compositions of the phenocrysts (and the temperatures calculated from them) but the homogeneity of individual mafic phenocrysts, and (5) the highly evolved character of the glass. Finally, this eruptive mixing model explains the anomalous WATER samples as glass-enriched products of a mixing of mafic phenocrysts with abundant silicic glass. Exactly when or how this mixing occurred is not constrained by the models. Mixing (without re-equilibration) could have occurred in the magma chamber during rapid withdrawal, during fragmentation in the conduit, or during pyroclastic flow and emplacement.

Certainly, these trace element models do not provide a unique solution but combine to suggest that progressive crystallization over a range of temperatures followed by eruptive mixing may explain much of the chemical and mineralogical variation in the tuff. Further studies of suites of pumices and of the trace element analyses of glass shards and glassy groundmasses may help constrain this evolutionary model for the Lund and for monotonous intermediates in general.

8. Geologic controls on the composition of the Lund Tuff

We next explore crustal thickness, rate of input of basaltic magma into the roots of the magma system, crustal stress distribution, and magma chamber shape as possible factors in the origin of the monotonous intermediate Lund magma.

8.1. Crustal thickness

Crustal thickness during the burst of Oligocene monotonous intermediate volcanism in the Great Basin can only be inferred indirectly because of subsequent east–west extension and consequent crustal thinning. The early Cenozoic crust had been thickened by Jurassic to Paleocene contractional orogenies to as much as an estimated 50–60

km (Jones et al., 1998; Zandt et al., 1995), compared to the current 25–35 km. Coney and Harms (1984) show a north–south trending 50–60 km thick crustal welt positioned along the Nevada–Utah stateline through the Indian Peak caldera complex (Fig. 17) and suggested (p. 553) that the eastern Great Basin "was a vast Tibetan or Andean altiplano plateau prior to middle-Tertiary crustal extension." Independent verification of a thick, early to middle-Tertiary crust is afforded by the compositions of the volcanic rocks of this age. In a comparison of subduction-related volcanic rocks worldwide (Barr, 1993), middle-Tertiary high-K lava flows in the Great Basin are compositionally most like Neogene rocks in the central Andean Altiplano–Puna and Oligocene rocks in the San Juan volcanic field. In these two volcanic fields, the thickness of the crust, which probably has not been modified significantly since volcanism, is currently 50–70 km (Allmendinger et al., 1997) and 48 km (Prodehl and Lipman, 1989), respectively. Comparisons of middle-Tertiary Great Basin rocks with the geochemical parameters of Leeman (1983) suggest the crust was 60–70 km thick; the magmas are markedly dissimilar to those erupted on thinner (<40 km) crust.

Thermal models of the effects of crustal thickening disclose peak elevation of temperature in the crust a few tens of millions of years after peak contraction (e.g., Huerta et al., 1996). For the area that is now the eastern Great Basin, major contractional deformation occurred about 90-60 Ma (DeCelles et al., 1995). Therefore, during the monotonous intermediate burst 31 to 27 Ma, lower and middle crustal temperatures were still likely elevated with respect to a normal geotherm, thereby facilitating crustal assimilation. However, thickened crust *alone* cannot account for generation of monotonous intermediate magmas. This is obvious from the fact that a mid-Tertiary amagmatic zone lies immediately south of the Great Basin ash-flow province in crust that is believed to have been 50–60 km thick (Fig. 17).

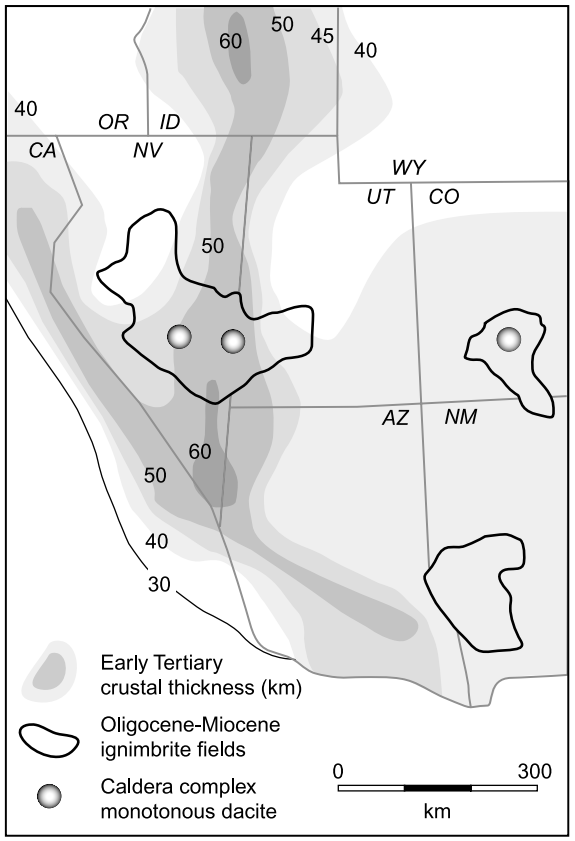

Fig. 17. Western US crustal thickness. Restored early Tertiary crustal thickness in what is now the Basin and Range province of the southwestern USA. Thickness contours at 30, 40, 45, 50, and 60 km from Coney and Harms (1984). The thickest crustal 'welt' reflects the effects of Mesozoic orogenies. The areas with bold outlines show Oligocene–Miocene ash-flow fields formed about 34–20 Ma. The Great Basin ash-flow province of Nevada and Utah includes the central Nevada and the Indian Peak caldera complexes (shaded) that were the source of four monotonous intermediate ash-flow tuffs, including the Lund Tuff. These caldera complexes formed where the ignimbrite belt intersected the thickest crust. The monotonous intermediate Fish Canyon Tuff in the southwestern Colorado San Juan volcanic field lies on somewhat thinner crust in this reconstruction (but currently about 48 km) whereas no monotonous intermediate tuffs occur in the southwestern New Mexico Mogollon–Datil volcanic field on still thinner crust.

8.2. Flux of mantle-derived mafic magma into the crust: magma generation

The critical heat source powering crustal magma generation has to be influx of mantle-derived mafic magma (e.g., Hildreth, 1981; Laube and Springer, 1998). In this area during the early to middle Tertiary, mafic magma was likely generated in the mantle wedge overlying subducting

oceanic lithosphere (Severinghaus and Atwater, 1990). Prior to the ignimbrite flareup, volcanic activity had swept southward through the northern Great Basin area (accompanying slab rollback) at a rate of about 50 km/Myr but during the flareup the sweep slowed to almost an order of magnitude less (Best and Christiansen, 1991). Thus, the ignimbrite flareup occurred in an arcuate, east-west zone across the central to southern Great Basin (Fig. 17) where there was a more focused influx of mafic magma into the crust. Monotonous intermediate magma generation occurred at the intersection of this east–west zone and the north–south-trending welt of most thickened crust (Coney and Harms, 1984).

O, Pb, Nd, and Sr isotopic data (Hart et al., 1998; Askren et al., 1997) indicate that substantial amounts of crustal rock, including upper crustal sediment, was assimilated into the mantle magma driving the silicic magma systems. For example, $\delta^{18}O$ in plagioclase separates from fifteen samples of the three Indian Peak monotonous intermediates is 7–9‰ (Hart, 1997), compared to a mantle value of 5.7 ± 0.3‰ and initial $^{87}Sr/^{86}Sr$ ranges to as high as 0.712 (Hart et al., 1998).

8.3. State of stress and crustal magma chamber shape

In the Great Basin, there is clear evidence for regional tectonic quiescence – neither extension nor contraction – during eruption of the monotonous intermediate tuffs (Best and Christiansen, 1991). The volume of mafic mantle-derived magma required to generate this huge volume of magma (e.g., Grunder, 1995) could not have been *entirely* emplaced as subvertical dikes because that would have produced significant horizontal crustal extension, for which there is no evidence. Rather, the magma was likely emplaced into the crust *mostly* as sills, necessarily fed from dikes tapping the mantle source. Magma chamber construction was probably accomplished by lifting the overlying crust against the least principal stress (σ_3), rather than forcing horizontally against the walls of dikes. Emplacement of mafic magma as sills rather than dikes efficiently releases more heat at a particular level and thus provides for more extensive melting of country rock (Huppert and Sparks, 1988). Stagnation of many basalt sills near the same crustal horizon could generate large volumes of dacitic magma by partial fusion of crustal rock and mixing with mantle-derived mafic magma. Existence of a plexus of basalt sills sufficient to drive silicic magma generation could be tested seismically.

The present-day Altiplano–Puna of the central Andes serves as analog of the middle-Tertiary Great Basin area. de Silva (1989) has proposed a similar scenario as just outlined for the late Miocene central Andean ignimbrite flareup. Isaaks (1988, p. 3228) postulated emplacement of sills during the Neogene into the crust and Allmendinger et al. (1997) envisage magmatic underplating contributing to plateau uplift. More direct seismic evidence for a flat slab of magma about 0.8 km thick underlying much of the central Altiplano–Puna at a depth of about 19 km has been documented by Chmielowski et al. (1999). They suggest it is a long-lived crustal storage zone replenished from deeper sources, perhaps lodged at the brittle–ductile transition (G. Zandt, 1999, written communication).

It seems likely, therefore, that the Lund magma was lodged in a flat sill, or perhaps a swarm of multiple sills. Such a configuration can account for the lack of significant compositional gradients in the Lund deposit. de Silva (1991) and de Silva and Wolff (1995) proposed that an important control on the degree of compositional variability in a pyroclastic deposit and in the pre-eruption magma chamber is its shape. In upright bottle-shaped chambers, significant sidewall crystallization yields less dense, fractionated residual melt which convectively buoys upward and collects as a layer of rhyolite magma at the top of the magma chamber (Fig. 18). However, in slab-like chambers, heat is lost chiefly through the roof but in thick slabs crystallization can occur at the floor as a result of the contrast in adiabatic and liquidus gradients. Cooling and densifying magma at the roof is negatively buoyant and tends to sink whereas floor crystallization releases less dense, compositionally buoyant, residual melt (e.g., Martin et al., 1987). Floor magma may also become thermally buoyant as it is heated by replenishing

hot magma from below. This buoyant magma would mix with the overlying magma rather than accumulating in a separate pool at the roof. The slab of magma is, therefore, stirred and mixed from above and below with the probable result that systematic, chamber-wide compositional and thermal gradients were limited in the milieu of rising and sinking plumes. A significant proportion of evolved rhyolitic melt could not segregate from crystals as in bottle-shaped chambers. Progressive crystallization would, nonetheless, occur causing mineral compositions to vary.

Even if compositional zoning existed in a slab-like chamber it would tend to be destroyed during eruption (S. De Silva, written communication, 1999), rather than preserved as in the systematic withdrawal of increasing diameter, deeper eruptive volumes of a zoned bottle-shaped chamber (e.g., Best et al., 1995, Fig. 18).

Therefore, despite the lack of systematic compositional gradients in the Lund Tuff, adjacent parcels of magma in a stirred magma slab could have varied somewhat in temperature, melt and mineral composition, and mode – even though the bulk composition of the parcels might have been similar. The lack of zoning in the mafic phenocrysts suggests that they remained in equilibrium with the melt in each parcel during crystallization. Possibly, there were multiple slab-like magma chambers of about the same bulk composition and each having evolved to a different degree that were tapped during the eruption.

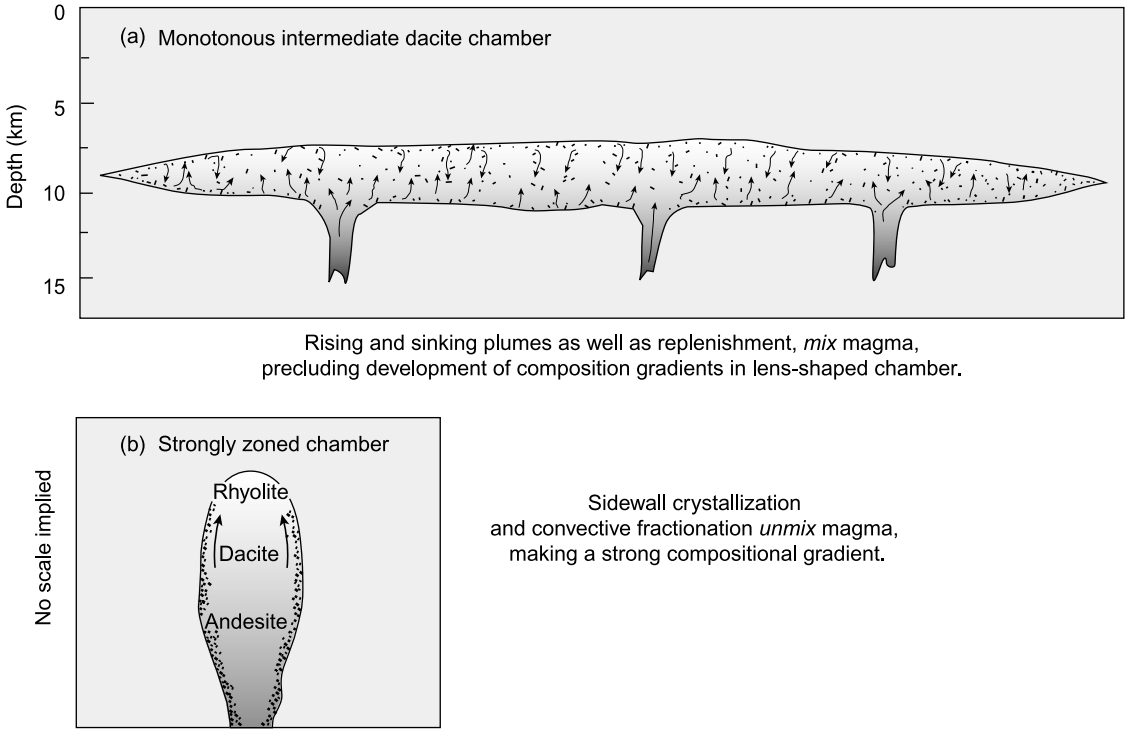

Fig. 18. Schematic contrast in magma evolution between an upright bottle-shaped magma chamber and a horizontal lens-shaped chamber. In the bottle-shaped chamber (depth scale unspecified), prominent sidewall fractional crystallization and associated thermochemical convection allows magma 'unmixing' and development of a differentiated rhyolitic cap. During evacuation from the top downward, chamber zonation is essentially preserved, but inverted, in the ignimbrite. In the hypothetical monotonous intermediate magma lens, sidewall crystallization is absent and development of a compositional gradient (especially of a separate body of evolved rhyolite magma) is limited because of convective stirring. Plumes of magma rise from the floor or fall from the roof as a result of density changes caused by crystallization and mix with the surrounding magma. Continued input of mafic magma stirs the pot as well. If any compositional or thermal gradients develop they tend to be erased during eruptive mixing and the resulting ignimbrite is compositionally heterogeneous but lacks systematic vertical or lateral zonation.

8.4. Eruptive aspects

The sill model for the Lund magma chamber would be consistent with rather wholesale evacuation at a high discharge rate. Perhaps, the 9 km thick roof of Precambrian and Phanerozoic quartzites and carbonate rocks (density about 2600–2800 kg/m^3) broke when it was no longer strong enough to span the >50 km diameter magma chamber. The roof would have subsided into the less dense (about 2450 kg/m^3) magma, forcing it out at a high rate. Relative to an end-member bottle-shaped chamber, a greater proportion of chamber magma might have been forced out. The large volume rate of eruption probably created a sustained collapsing pyroclastic fountain (Sparks et al., 1997) from which ash flows spread laterally for great distances.

9. Conclusions

The dacitic Lund Tuff is a very large volume ash-flow deposit in the Indian Peak volcanic field of the Oligocene Great Basin ignimbrite province. It is a distinctive monotonous intermediate tuff. The tuff contains abundant phenocrysts of (in generally decreasing amounts) plagioclase, quartz, hornblende, biotite, sanidine, Fe–Ti oxides, and titanite. It was emplaced at 29.02 ± 0.04 Ma, has a normal paleomagnetic direction, and has an estimated volume of at least 2900–3600 km^3 (adjusted for 30–70% uniform post-volcanic crustal extension; 2600–3200 km^3 on a dense rock basis). The White Rock caldera has a north–south unextended dimension of about 50 km. The Silver King tuff, which was originally included with the Lund Tuff stratigraphic unit, is older (29.22 ± 0.03 Ma), reversely polarized, an order of magnitude smaller in volume, and compositionally distinct.

The Lund Tuff is compositionally monotonous – it has virtually the same phenocryst assemblage throughout; it lacks systematic compositional zonation; and it lacks an underlying co-genetic rhyolitic precursor or precursory plinian fallout. Nonetheless, there are significant variations in bulk-rock compositions and in proportions and compositions of phenocrysts, all of which vary along normal calc-alkaline differentiation trends. The tuff typically has 40–50% phenocrysts and cognate pumice fragments are similarly phenocryst-rich.

We postulate that the distinctive attributes of the Lund Tuff, resulted from the following factors:

1. The coincidence of unusually warm orogenically thickened crust and an unusually high flux of mafic mantle magma generated during roll back of a subducting slab combined to enhance crustal melting and assimilation. This created a very large volume of dacitic magma.
2. This magma accumulated in a flat sill-like chamber about 50 km across at a depth of about 9 km. Sills were the dominant shape in this thick crust under the quasi-hydrostatic state of stress that prevailed during the middle Tertiary in the Great Basin.
3. *Convective mixing* in the sill precluded development of a strong chamber-wide compositional gradient that could be inverted systematically upon eruption (as occurs in chambers where extensive sidewall crystallization and *convective fractionation* create a cap of evolved rhyolite magma).
4. Nonetheless, varying temperatures in the chamber created separate magma parcels that experienced different degrees of equilibrium crystallization. Each parcel had its own distinctive temperature (730–800°C), phenocryst proportions, and mineral compositions.
5. Fragmentation and physical mixing of glass and phenocrysts from these parcels occurred during evacuation and eruption and created a range of tuff compositions.
6. The large size of the chamber combined with roof subsidence created high mass eruption rates and a continuously collapsing eruption cloud. No plinian fallout preceded the eruption.
7. Separation of glass from phenocrysts was not a major factor in creating the compositional spectrum.

Acknowledgements

Funding for our study of Great Basin volcanism was provided by NSF Grants EAR-8604195, 8904245, and 9104612, 9706906, by BYU, and by the Lewis stipend for graduate student research in igneous petrology at BYU. Helpful comments on early versions of the manuscript by Anita Grunder, Peter Lipman, and Shan de Silva clarified our presentation.

References

Allmendinger, R.W., Jordan, T.E., Kay, S.M., Isacks, B.L., 1997. The evolution of the Altiplano-Puna plateau of the central Andes. Annu. Rev. Earth Planet. Sci. 25, 139–174.

Anderson, J.L., Smith, D.R., 1995. The effects of temperature and fO_2 on the A1-inhornblende barometer. Am. Mineral. 89, 549–559.

Askren, D.R., Roden, M.F., Whitney, J.A., 1997. Petrogenesis of andesite lava flows interlayered with large-volume felsic ash-flow tuffs in the western USA. J. Petrol. 38, 1021–1046.

Bacon, C.R., Hirschmann, M.M., 1988. Mg/Mn partitioning as a test for equilibrium between coexisting Fe-Ti oxides. Am. Mineral. 73, 57–61.

Barr, D.L., 1993. Time, Space, and Composition Patterns of Middle Cenozoic Mafic to Intermediate Composition Lava Flows of the Great Basin, Western U.S.A. M.S. Thesis, Brigham Young University, Provo, UT, 68 pp.

Best, M.G., Christiansen, E.H., 1991. Limited extension during peak Tertiary volcanism, Great Basin of Nevada and Utah. J. Geophys. Res. 96, 13509–13528.

Best, M.G., Christiansen, E.H., 1997. Origin of broken phenocrysts in ash-flow tuffs. Geol. Soc. Am. Bull. 109, 63–73.

Best, M.G., Christiansen, E.H., Blank, H.R., Jr., 1989a. Oligocene caldera complex and calc-alkaline tuffs and lavas of the Indian Peak volcanic field, Nevada and Utah. Geol. Soc. Am. Bull. 101, 1076–1090.

Best, M.G., Christiansen, E.H., Deino, A.L., Grommé, C.S., McKee, E.H., Noble, D.C., 1989b. Eocene through Miocene volcanism in the Great Basin of the western United States. New Mex. Bur. Mines Miner. Res. Mem. 47, 91–133.

Best, M.G., Christiansen, E.H., Deino, A.L., Grommé, C.S., Tingey, D.G., 1995. Correlation and emplacement of a large, zoned, discontinuously exposed ash-flow sheet: $^{40}Ar/^{39}Ar$ chronology, paleomagnetism, and petrology of the Pahranagat Formation, Nevada. J. Geophys. Res. 100, 24593–24609.

Best, M.G., Hintze, L.F., Deino, A.L., Maughan, L.L., 1998. Geologic map of the Fairview Range and Grasy Mountain, Lincoln County, Nevada. Nevada Bur. Mines Geol. Map 114.

Best, M.G., Scott, R.B., Rowley, P.D., Swadley, W C, Anderson, R.E., Grommé, C.S., Harding, A.E., Deino, A.L., Christiansen, E.H., Tingey, D.G., Sullivan, K.R., 1993. Oligocene-Miocene caldera complexes, ash-flow sheets, and tectonism in the central and southeastern Great Basin. In: Lahren, M.M., Trexler, J.H., Jr. (Eds.), Crustal Evolution of the Great Basin and the Sierra Nevada. Geol. Soc. Am. Field Trip Guidebook, pp. 285–312.

Bohlen, S.R., Peacor, D.R., Essene, E.J., 1980. Crystal chemistry of a metamorphic biotite and its significance on water barometry. Am. Mineral. 65, 55–62.

Chmielowski, J., Zandt, G., Haberland, C., 1999. The central Andean Altiplano-Puna magma body. Geophys. Res. Lett. 26, 783–786.

Christiansen, E.H., Burt, D.M., Sheridan, M.F., Wilson, R.T., 1983. Petrogenesis of topaz rhyolites from the western United States. Contrib. Mineral. Petrol. 83, 16–30.

Coney, P.J., Harms, T.A., 1984. Cordilleran metamorphic core complexes: Cenozoic extensional relics of Mesozoic compression. Geology 12, 550–554.

DeCelles, P.G., Lawton, T.F., Mitra, G., 1995. Thrust timing, growth of structural culminations, and synorogenic sedimentation in the type Sevier orogenic belt, western United States. Geology 23, 699–702.

de Silva, S.L., 1989. Geochronology and stratigraphy of ignimbrites from the 21°30′ to 23°30′S portion of the central Andes of N. Chile. J. Volcanol. Geotherm. Res. 37, 93–131.

de Silva, S.L., 1991. Styles of zoning in central Andean ignimbrites: Insights into magma chamber processes. Geol. Soc. Am. Spec. Pap. 265, 217–232.

de Silva, S.L., Wolff, J.A., 1995. Zoned magma chambers: The influence of magma chamber geometry on sidewall convective fractionation. J. Volcanol. Geotherm. Res. 65, 111–118.

Diehl, J.F., Beck, M.E., Jr., Beske-Diehl, S., Jacobson, D., Hearn, B.C., Jr., 1983. Paleomagnetism of the Late Cretaceous-Early Tertiary north-central Montana alkalic province. J. Geophys. Res. 88, 10593–10609.

Ekren, E.B., Anderson, R.E., Rogers, C.L., Noble, D.C., 1971. Geology of the Northern Nellis Air Force Base Bombing and Gunnery Range, Nye County, Nevada. U.S. Geol. Surv. Prof. Pap. 651, 91 pp.

Ekren, E.B., Page, W.R., 1995. Preliminary Geologic Map of the Coyote Spring Quadrangle, Lincoln County, Nevada. U.S. Geol. Surv. Open-File Report 95-550, 19 pp.

Fisher, R.A., 1953. Dispersion on a sphere. Proc. R. Soc. London A 217, 295–305.

Francis, P.W., Sparks, R.S.J., Hawkesworth, C.J., Thorpe, R.S., Pyle, D.M., Tait, S.R., Mantovani, M.S., McDermott, F., 1989. Petrology and geochemistry of volcanic rocks of the Cerro Galan caldera, northwest Argentina. Geol. Mag. 126, 515–547.

Fuhrman, M.L., Lindsley, D.H., 1988. Ternary-feldspar modeling and thermometry. Am. Mineral. 73, 201–215.

Ghiorso, M.S., Sack, R.O., 1991. Fe-Ti oxide geothermometry: Thermodynamic formulation and the estimation of in-

tensive variables in silicic magmas. Contrib. Mineral. Petrol. 108, 485–510.

Grommé, C.S., McKee, E.H., Blake, M.C., Jr., 1972. Paleomagnetic correlations and potassium-argon dating of middle-Tertiary ash-flow sheets in the eastern Great Basin, Nevada and Utah. Geol. Soc. Am. Bull. 83, 1619–1638.

Grunder, A.L., 1995. Material and thermal roles of basalt in crustal magmatism: case study from eastern Nevada. Geology 23, 952–956.

Hart, G.L., 1997. An Oxygen Isotope Investigation of the Indian Peak Volcanic Field, Southern Utah-Nevada: Magma Source Constraints for a Late Oligocene Caldera System. M.S. Thesis, Brigham Young University, Provo, UT, 57 pp.

Hart, G.L., Johnson, C.M., Beard, B.L., Christiansen, E.H., Best, M.G., 1998. Evidence of crustal interaction for the Oligocene Indian Peak and Central Nevada caldera complexes, as deduced from Pb isotope data. Geol. Soc. Am. Prog. Abstr. 30, no. 7, p. A-90.

Hildreth, W., 1979. The Bishop Tuff: Evidence for the origin of compositional zonation in silicic magma chambers. Geol. Soc. Am. Spec. Pap. 180, 43–75.

Hildreth, W., 1981. Gradients in silicic magma chambers: Implications for lithospheric magmatism. J. Geophys. Res. 86, 10153–10192.

Holland, T., Blundy, J., 1994. Non-ideal interactions in calcic amphiboles and their bearing on amphibole-plagioclase thermometry. Contrib. Mineral. Petrol. 116, 433–447.

Huerta, A.D., Royden, L.H., Hodges, K.V., 1996. The interdependence of deformation and thermal processes in mountain belts. Science 273, 637–639.

Huppert, H.E., Sparks, R.S.J., 1988. The generation of granitic magmas by intrusion of basalt into continental crust. J. Petrol. 29, 599–624.

Isaaks, B.L., 1988. Uplift of the central Andean plateau and bending of the Bolivian orocline. J. Geophys. Res. 93, 3211–3231.

Johnson, M.C., Rutherford, M.J., 1989a. Experimental calibration of the aluminum-in-hornblende geobarometer with application to Long Valley caldera (California) volcanic rocks. Geology 17, 837–841.

Johnson, M.C., Rutherford, M.J., 1989b. Experimentally determined conditions in the Fish Canyon Tuff, Colorado, magma chamber. J. Petrol. 30, 711–737.

Jones, C.H., Sonder, L.J., Unruh, J.R., 1998. Lithospheric gravitational potential energy and past orogenesis: Implications for conditions of initial Basin and Range and Laramide deformation. Geology 26, 639–642.

Kirschvink, J.L., 1980. The least squares line and plane and analysis of paleomagnetic data. Geophys. J. R. Astron. Soc. 62, 699–718.

Laube, N., Springer, J., 1998. Crustal melting by ponding of mafic magmas: A numerical model. J. Volcanol. Geotherm. Res. 81, 19–35.

Leeman, W.P., 1983. The influence of crustal structure on compositins of subduction-related magmas. J. Volcanol. Geotherm. Res. 18, 561–588.

LeMaitre, R.W., 1989. A Classification of Igneous Rocks and Glossary of Terms. Blackwell Scientific, Oxford, 193 pp.

Lipman, P.W., 1975. Evolution of the Platoro Caldera Complex and Related Volcanic Rocks, Southeastern San Juan Mountains. U.S. Geol. Surv. Prof. Pap. 852, 127 pp.

Lipman, P.W., 1997. Subsidence of ash-flow calderas: Relation to size and magma chamber geometry. Bull. Volcanol. 59, 198–218.

Lipman, P.W., 2000. The central San Juan caldera cluster: Regional volcanic framework. Geol. Soc. Am. Spec. Pap. 346, 9–69.

Lipman, P.W., Dungan, M.A., Bachmann, O., 1997. Comagmatic granophyric granite in the Fish Canyon Tuff, Colorado: Implications for magma-chamber processes during a large ash-flow eruption. Geology 25, 915–918.

Luhr, F.J., Carmichael, I.S.E., Varekamp, J.C., 1984. The 1982 eruptions of El Chichón volcano, Chiapas, Mexico: Mineralogy and petrology of the anhydrite-bearing pumices. J. Volcanol. Geotherm. Res. 23, 69–108.

Martin, D., Griffiths, R.W., Campbell, I.H., 1987. Compositional and thermal convection in magma chambers. Contrib. Mineral. Petrol. 96, 465–475.

Maughan, L.L., 1996. Petrology and Eruptive History of the Dacitic Ash-flow Tuffs of the Lund Formation, Southeastern Nevada and Southwestern Utah. M.S. Thesis, Brigham Young University, Provo, UT, 54 pp.

McDonough, W.F., Sun, S.S., 1995. The composition of the Earth. Chem. Geol. 120, 223–253.

Pearce, J.A., Harris, N.B., Tindle, A.G., 1984. Trace element discrimination diagrams for the tectonic interpretation of granitic rocks. J. Petrol. 25, 956–983.

Phillips, L.V., 1989. The Petrology and Magmatic Evolution of the Large-volume Ash-flow Tuffs of the Central Nevada Caldera Complex, Nye County, Nevada. Ph.D. Thesis, University of Georgia, Athens, GA, 285 pp.

Prodehl, C., Lipman, P.W., 1989. Crustal structure of the Rocky Mountain region. Geol. Soc. Am. Mem. 172, 249–284.

Renne, P.R., Swisher, C.C., Deino, A.L., Karner, D.B., Owens, T.L., DePaolo, D.J., 1998. Intercalibration of standards, absolute ages and uncertainties in $^{40}Ar/^{39}Ar$ dating. Chem. Geol. 145, 117–152.

Rollinson, H., 1993. Using Geochemical Data. Longman Group, Harlow, 352 pp.

Scott, R.B., Grommé, C.S., Best, M.G., Rosenbaum, J.G., Hudson, M.R., 1995. Stratigraphic relationships of Tertiary volcanic rocks in central Lincoln County, southeastern Nevada. U.S. Geol. Surv. Bull. 2056-A, 7–41.

Severinghaus, J., Atwater, T., 1990. Cenozoic geometry and thermal state of the subducting slabs beneath western North America. Geol. Soc. Am. Mem. 176, 1–22.

Smith, D.L., Gans, P.B., Miller, E.L., 1991. Palinspastic restoration of Cenozoic extension in the central and eastern Basin and Range province at latitude 39–40°N. In: Raines, G.L., Lisle, R.E., Schafer, R.W., Wilkinson, W.H. (Eds.), Geology and Ore Deposits of the Great Basin. Geol. Soc. Nevada, pp. 75–86.

Sparks, R.S.J., Bursik, M.I., Carey, S.N., Gilbert, J.S., Glaze, L.S., Sigurdsson, H., Woods, A.W., 1997. Volcanic Plumes. John Wiley and Sons, New York, 574 pp.

Stormer, J.C., Nicholls, J., 1978. XLFRAC: A program for the interactive testing of magmatic differentiation models. Comput. Geosci. 4, 143–159.

Taylor, S.R., McLennan, S.M., 1985. The Continental Crust: its Composition and Evolution. Blackwell, Oxford.

Whitney, J.A., Stormer, J.C., Jr., 1985. Mineralogy, petrology, and magmatic conditions from the Fish Canyon Tuff, central San Juan Volcanic Field, Colorado. J. Petrol. 26, 726–762.

Wones, D.R., 1989. Significance of the assemblage titanite+ magnetite+quartz in granitic rocks. Am. Miner. 74, 744–749.

Zandt, G., Myers, S.C., Wallace, T.C., 1995. Crust and mantle structure across the Basin and Range-Colorado Plateau boundary at 37°N latitude and implications for Cenozoic extensional mechanism. J. Geophys. Res. 100 m, 10529–10548.